Volume 27
Number 26
14 July 2025
Pages 4417–4606

CrystEngComm

rsc.li/crystengcomm

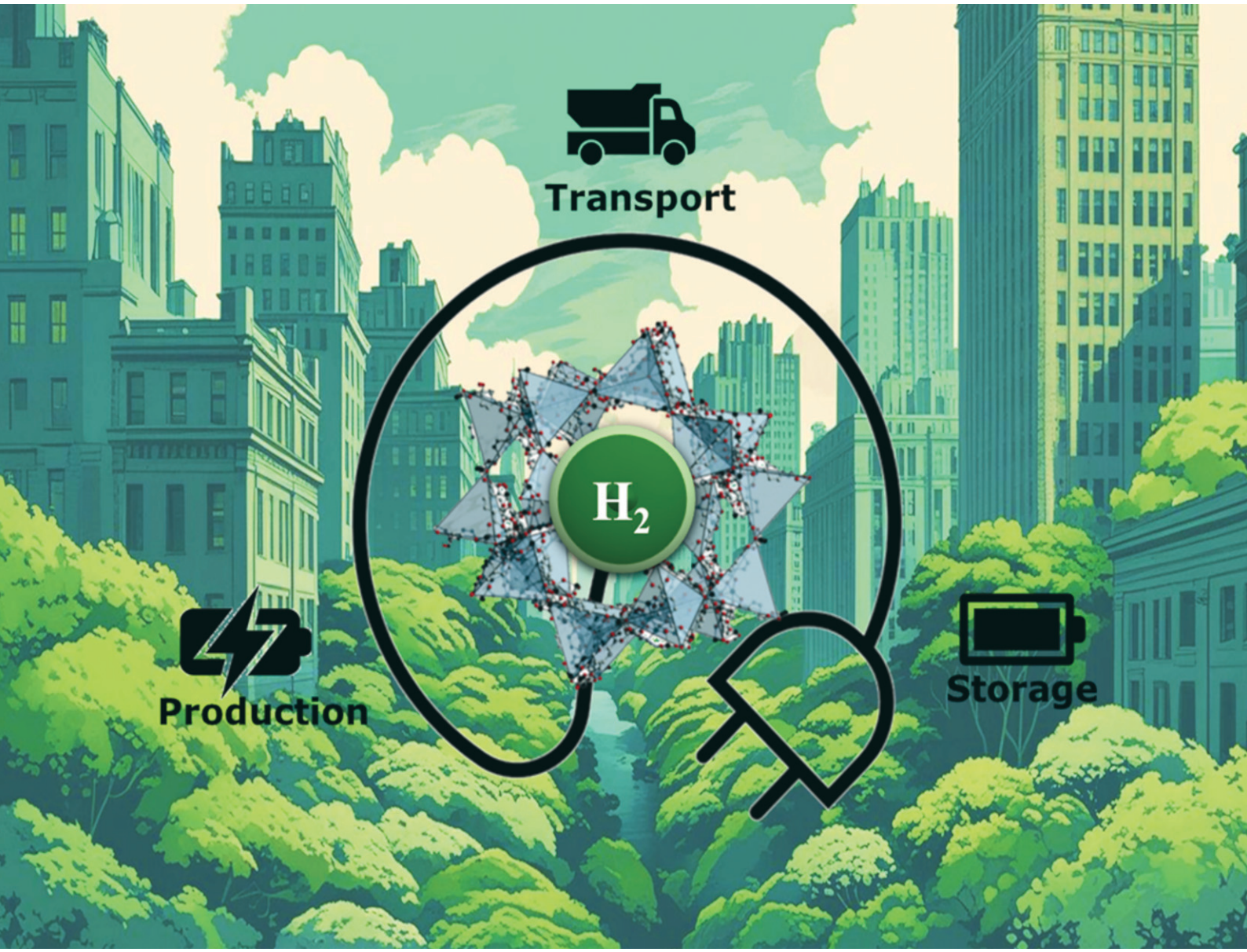

ISSN 1466-8033

ROYAL SOCIETY OF CHEMISTRY

HIGHLIGHT
Eduardo Schott *et al.*
MOFs as a partner for the H_2 industry

CrystEngComm

HIGHLIGHT

View Article Online
View Journal | View Issue

Cite this: *CrystEngComm*, 2025, **27**, 4425

MOFs as a partner for the H_2 industry

Javier Salazar-Muñoz,[a] Yazmin Arellano,[a] Vanesa Roa,[a] Gabriel Bernales,[a] Diego Gonzalez,[a] Yoan Hidalgo-Rosa,[bc] Ximena Zarate[d] and Eduardo Schott *[a]

Metal–organic frameworks (MOFs) are hybrid organic–inorganic porous materials composed of transition metal cations and polydentate organic ligands, forming modular architectures with high porosity and surface areas. These properties make MOFs promising candidates for hydrogen (H_2) storage and production, catalysis, sensing and gas separation, among others. Since their conceptualization in 1995 by Omar Yaghi, MOFs have evolved significantly, with over 100 000 types reported, exhibiting surface areas ranging from 500 to 8000 $m^2\ g^{-1}$. Their structural versatility, governed by secondary building units (SBUs) and ligand geometries, allows for tailored pore sizes and functionalities, critical for optimizing H_2 storage. MOFs with open metal sites (OMSs) enhance H_2 adsorption by providing stronger binding sites, while advancements in synthesis methods, such as solvothermal, microwave, and spray drying methods, have improved scalability and efficiency. Recent developments include MOF composites and bimetallic frameworks, which exhibit synergistic effects for enhanced H_2 storage and catalytic performance. For instance, NU-1501 achieves a H_2 gravimetric capacity of 14 wt%, while bimetallic MOFs like Zr/Hf-UiO-66 demonstrate superior catalytic activity. Additionally, MOFs are being explored for H_2 production *via* electrocatalysis and photocatalysis, leveraging their tunable electronic properties and high surface areas. Despite challenges in scalability and stability, startups like H_2MOF and Rux Energy are pioneering MOF-based H_2 storage solutions, aiming to meet the U.S. Department of Energy targets for on-board H_2 storage. Computational modeling and reticular chemistry further accelerate the design of MOFs with optimized H_2 storage capacities, paving the way for their integration into sustainable energy systems. While commercial applications remain limited, ongoing research and industrial collaborations continue to advance MOFs toward practical H_2 storage and energy conversion technologies.

Received 8th April 2025,
Accepted 29th May 2025

DOI: 10.1039/d5ce00384a

rsc.li/crystengcomm

Introduction

Rapid industrialization has played a crucial role in driving economic wealth and population growth, leading to technological advancements, improved infrastructure, and higher living standards. However, this rapid expansion has also resulted in severe environmental consequences, including rising greenhouse gas emissions, escalating global temperatures, and increasing energy shortages.[1,2] One of the most pressing challenges is climate change, which has led to extreme weather patterns, melting ice caps, and rising sea levels, posing serious threats to ecosystems and human societies worldwide.[3]

To combat the adverse effects of climate change, there has been a growing global initiative to implement rigorous environmental policies aimed at reducing greenhouse gas emissions. Many countries have set ambitious targets to transition towards cleaner and more sustainable energy sources. For instance, France enacted Law No. 2015-992, which mandates a 40% reduction in greenhouse gas emissions by 2030 compared to 1990 levels.[4] This legislation reflects a broader international commitment to mitigating climate change through policy-driven efforts, increased investment in renewable energy, and technological innovations that promote energy efficiency.

While various factors contribute to greenhouse gas emissions, the burning of fossil fuels remains the primary culprit. Coal, oil, and natural gas have long been the pillars of industrial growth and energy production, but their extensive use has led to massive carbon dioxide emissions,

[a] *Departamento de Química Inorgánica, Facultad de Química y de Farmacia, Centro de Energía UC, Centro de Investigación en Nanotecnología y Materiales Avanzados CIEN-UC, Pontificia Universidad Católica de Chile, Vicuña Mackenna 4860, Macul, 7820436 Santiago, Chile. E-mail: maschotte@gmail.com, edschott@uc.cl*
[b] *Centro de Nanotecnología Aplicada, Facultad de Ciencias, Ingeniería y Tecnología, Universidad Mayor, Camino La Pirámide 5750, Huechuraba, Santiago, Chile*
[c] *Escuela de Ingeniería del Medio Ambiente y Sustentabilidad, Facultad de Ciencias, Ingeniería y Tecnología, Universidad Mayor, Camino La Pirámide 5750, Huechuraba, 8580745 Santiago, Chile*
[d] *Instituto de Ciencias Aplicadas, Facultad de Ingeniería, Universidad Autónoma de Chile, Av. Pedro de Valdivia 425, Santiago, Chile*

exacerbating global warming. According to the United States Environmental Protection Agency (EPA), fossil fuel combustion is responsible for approximately 76% of all U.S. emissions resulting from human activities.[5] This alarming statistic underscores the urgent need to transition away from fossil fuel dependency and embrace cleaner alternatives such as wind, solar, and H_2-based energy systems.[6]

As nations continue to grapple with the dual challenge of sustaining economic growth while reducing environmental harm, see Fig. 1, it is imperative to accelerate the adoption of sustainable energy solutions and reinforce policies that promote carbon neutrality. The path forward requires a collaborative effort between governments, industries, and individuals to create a cleaner and greener future for generations to come.

To address the pressing challenges of climate change and the growing energy crisis, it is imperative to explore alternative clean energy sources and gradually transition away from traditional fossil fuels such as oil and coal. These conventional energy sources, while historically essential for industrialization and economic growth, have significantly accelerated the environmental decline in a considerable way in the last decades. As global energy demands continue to rise, finding sustainable and carbon-neutral alternatives has become a priority for researchers, policymakers, and industries equally.

Among the various emerging energy solutions, H_2 has garnered considerable attention as one of the most promising candidates for a sustainable energy transition. H_2 offers several key advantages that make it an attractive alternative to fossil fuels. It boasts an exceptionally high energy density of approximately 142 MJ kg^{-1} (gasoline has 46 MJ kg^{-1} for example), making it a highly efficient energy carrier. Moreover, H_2 is an environmentally friendly option, as it produces only water as a by-product when used in fuel cells.[8] Additionally, H_2 can be derived from a variety of renewable sources, including water electrolysis powered by solar, wind, or hydroelectric energy, further reinforcing its potential as a clean and sustainable fuel.[9–11]

Despite its potential, the widespread adoption of H_2 as a primary energy source faces significant challenges, particularly in its generation and storage. H_2 gas is highly reactive and has a low volumetric density, making its storage and transportation complex and costly. Traditional storage methods, such as compression and liquefaction, require high pressures and extremely low temperatures, increasing both energy consumption and operational costs. Additionally, H_2 production methods, including steam methane reforming (SMR) and water electrolysis, still face efficiency and cost barriers that hinder large-scale implementation.[11] Several reports cover the implementation of different kinds of catalysts to produce H_2.[12–14] In general, these catalysts could be homogeneous, heterogeneous or biocatalysts. The selection of a catalyst is based on the synthesis method selected to produce H_2. The main limitation of these catalysts arose from the cost associated with their production and modification.

To overcome these challenges, metal–organic frameworks (MOFs) have emerged as a promising alternative for both H_2 storage and generation. MOFs are highly porous materials with tunable structures, offering exceptional surface area and gas adsorption properties. These characteristics make them ideal candidates for efficiently storing H_2 at lower pressures and ambient temperatures, thereby addressing the limitations of conventional storage technologies. Additionally, recent research has explored MOFs as catalysts for H_2 production, providing new pathways to enhance the efficiency and sustainability of H_2 generation. By leveraging MOFs, the H_2 economy can move closer to achieving practical, scalable, and cost-effective energy solutions.[5] One

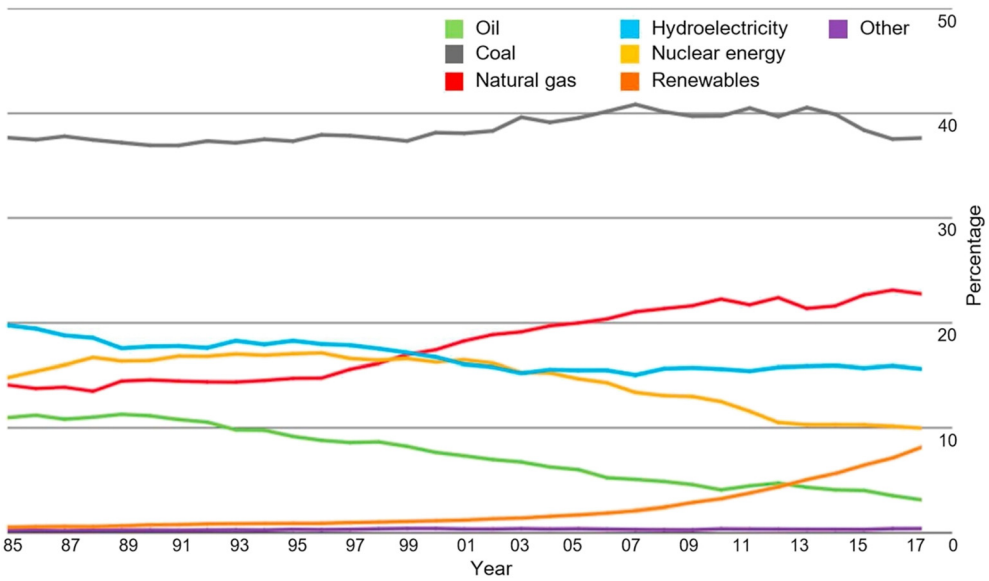

Fig. 1 Global electricity generation source. Adapted from ref. 7. Copyright 2024 ScienceDirect.

of the most remarkable properties of MOFs is their tunable electronic properties, which can be modulated by adjusting the metal centers in the nodes or the organic ligands that serve as linkers.[15]

From a technoeconomic perspective, the current state of H_2 storage and generation still struggles to compete with conventional fossil fuels in terms of cost-effectiveness and infrastructure readiness. The high production and storage costs remain key obstacles to the widespread commercialization of H_2 energy. Therefore, advancing technologies that can reduce these costs is crucial to making H_2 a viable competitor in the global energy market. MOFs, with their ability to enhance storage efficiency and production processes, represent a cutting-edge solution that could drive the H_2 economy forward. Continued research, investment, and policy support are necessary to refine these technologies and pave the way for a cleaner and more sustainable energy future.[9]

Among the various applications of H_2 storage technology, the automotive sector presents the greatest challenge. Unlike portable electronic devices such as laptops and mobile phones, which can efficiently utilize compact fuel cells for power generation, H_2 storage for vehicles requires significantly larger energy capacities and must meet stringent safety, efficiency, and economic viability standards. Similarly, while non-automotive transportation applications, such as motorbikes and small-scale H_2-powered transportation, have shown promise, the large-scale adoption of H_2 as a fuel for automobiles remains a critical hurdle due to the complexities associated with storage, infrastructure, and cost-effectiveness.[16]

Research and development in H_2 storage technology have been ongoing for several decades, with numerous breakthroughs aimed at enhancing H_2 storage efficiency, safety, and scalability.[9] Scientists and engineers have explored various storage methods, including high-pressure gas cylinders, cryogenic liquid H_2 storage, and solid-state H_2 storage using advanced materials. Among these, nanoporous materials such as MOFs have attracted particular attention due to their high surface area, tunable porosity, and superior H_2 adsorption capabilities. MOFs offer a promising alternative for efficient H_2 storage, potentially enabling vehicles to store sufficient H_2 for long-range travel while maintaining safety and cost efficiency.[1,17–19]

To date, a substantial body of research has reviewed the applications and future directions of H_2 storage materials, including nanoporous H_2 storage materials and MOFs. These reviews have highlighted the technological advancements and limitations of existing materials, providing valuable insights into their potential for real-world applications. However, despite these extensive studies, a detailed structural analysis of MOFs, focusing on the relationship between their framework architecture and H_2 storage capabilities, remains lacking. Understanding this structure–activity relationship is crucial for optimizing MOFs to achieve higher H_2 uptake, improved stability, and enhanced adsorption/desorption kinetics.

In this report, we aim to provide a comprehensive analysis of the latest developments in MOFs for H_2 generation, storage, and real-life applications related to their structures. Our focus is to bridge the gap between material design and practical implementation by thoroughly examining how structural modifications in MOFs influence their H_2 storage and generation performance. By shedding light on the fundamental mechanisms governing H_2 interactions within MOFs, this report will contribute to advancing the field and paving the way for the next generation of efficient and scalable H_2 storage solutions.

Structure of a MOF

MOFs are a class of hybrid organic–inorganic porous materials, also called coordination complex polymers. MOFs are composed of transition metal cations and polydentate organic ligands with carboxylate, sulfonate, imidazolate and other ionic groups.[20] These organic ligands bind orderly to the coordination sphere of metal cations replicating in space, resulting in modular architectures, with different topologies conferring a large internal surface area and high porosity. These topological characteristics of MOFs coupled with their low density, high surface adaptability such as pore size and changes in their active sites have made them interesting and promising heterogeneous catalysts, adsorbing and storing materials for different gases such as CO_2, short chain hydrocarbons, or H_2.[21,22]

These organic–inorganic materials were initially developed in 1989 by Richard Robert,[23] who synthesized a three-dimensional coordination polymer $[Cu[C(C_6H_4CN)_4]]_n^{n+}$, but it was not until 1995 when Omar Yaghi first introduced the concept of MOFs.[24] In this report, he developed MOF-5 composed of terephthalic acid and zinc, which presented a high pore volume and great thermal stability, and was a good candidate for H_2 and methane storage. This finding was an achievement for reticular chemistry in the development of organometallic materials, since it was thought that these materials could only adopt amorphous structures, therefore, the advances in MOF synthesis opened a new window towards the formation of materials with high porosity. Currently, about 100 000 types of MOFs have been reported where their surface areas vary between 500 and 8000 $m^2\ g^{-1}$, with narrow pore size distribution and low bulk density, which make them good candidates for H_2 storage.

The main structural characteristics of MOFs that provide them with high porosity and surface area are the different topologies that these materials acquire, so it is very important to decipher and understand their complex structure for the design of new MOFs and to understand how their surface and porosity can be modified to improve their H_2 storage properties. By analyzing the topology of a MOF and unraveling its structure, a repetitive unit known as secondary building units (SBUs) is defined,[25] which (as its

name implies) is the building block that by the repetition of this unit shapes the structure of a MOF. SBUs correspond to the metal clusters that adopt different geometries depending on the coordination number of the metal node and the anionic group of the used linker. SBUs are classified according to their points of extension (POEs), which mean the number of possible connectors that can link an SBU to other SBUs through linkers. Fig. 2 shows some carboxyl-based SBUs commonly found in MOFs. Each SBU adopted a different geometry and form, which depends on the sphere of coordination of the metal cation used. Each carbon atom of the carboxylic group in the SBUs represents a point of extension (POE) to connect with another SBU where the minimum number of POEs is 3 and the maximum is 18.[26,27] Therefore, to understand the SBU geometry using POEs, each carbon atom is taken as a vertex and is connected by edges with the other carbon atoms in the SBU, everything inside the vertices is represented by a green area. The shape of the metal cluster SBU is defined by the number and position of POEs in the SBU. For example, SBU $M_2(–COO)_4$ (M = Zn and Cu) has POEs of four with a square paddlewheel SBU geometry. If the $M_2(–COO)_4$ SBU uses a carboxylic acid ligand such as benzene-1,4-dicarboxylic acid (H_2BDC) and is replicated in a 2 dimension, MOF-2 is obtained, which has a 2D structure. On the other hand, if the $M_2(–COO)_4$ SBU uses a benzene-1,3,5-tricarboxylate (H3BTC) linker, HKUST-1 is obtained, which is a 3D MOF. Although the topology of the MOFs is different, they both have the same square paddlewheel SBU geometry.[28,29]

Each SBU can be composed of different numbers of metals (from 1 to 6). Knowing the SBU that can form a metal cation with a type of organic ligand, different types of MOFs can be designed with different topologies by varying the geometry of the used ligand.[6,7] For example, in Fig. 3, the SBU $Zn_4O(–COO)_6$ formed from Zn(II) and a carboxylic acid ligand is shown, this SBU has POEs of 6 and an octahedral geometry, and depending on the carboxylic acid ligand employed to construct this SBU (terephthalic acid (H_2BDC), 1,4-naphthalenedicarboxylic acid (H_2NDC), or 4,4-biphenyldicarboxylic acid (H_2BPDC)), different MOFs can be obtained, MOF-5, UMCM-8, DUT-6, and MOF-177, which will have different topologies, internal surface areas and pore volumes, and therefore will have different applicabilities.[31–33] Thus, knowing the SBU is of utmost importance to define the construction of a MOF, since the topology of the MOF is defined by the SBU formed and the geometry of the ligand used. This knowledge is crucial for the construction of MOFs used as H_2 storage, since some topologies will be more efficient than others for higher storage capacity.[34,35]

The stability of the MOFs under different conditions will depend on many factors, such as the rigidity of the ligand, the geometry of the metal coordination sphere, and the

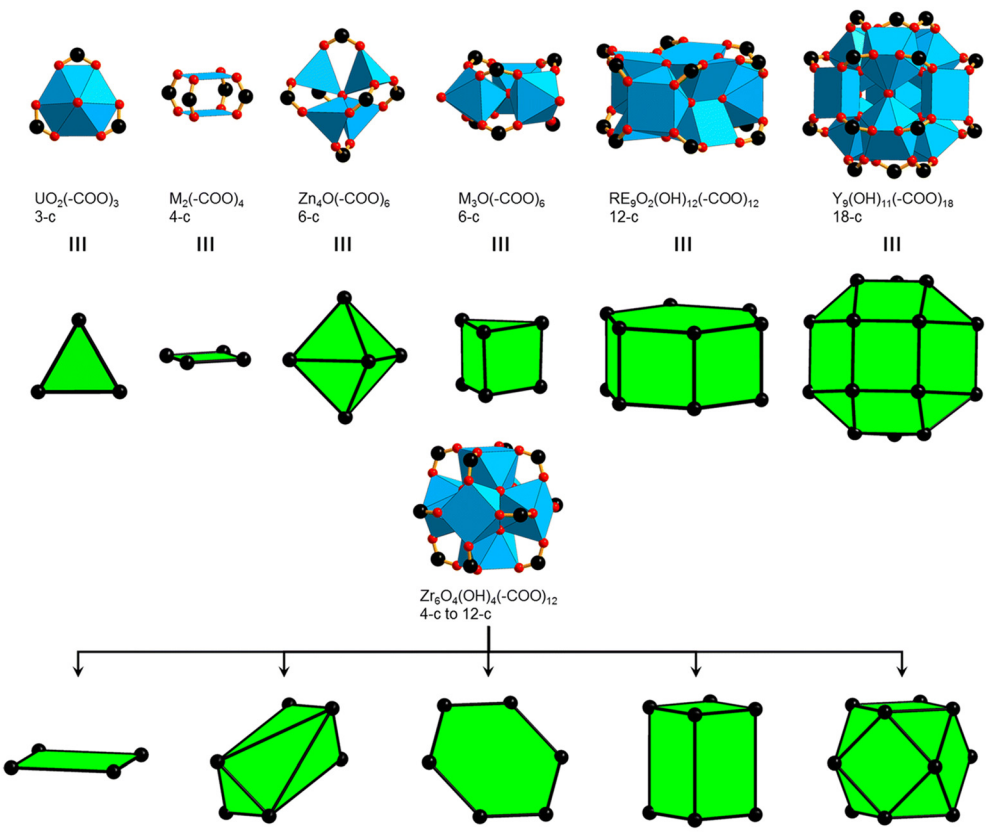

Fig. 2 Common metal secondary building units (SBUs) to construct MOFs. Color code: black, C; red, O; blue polyhedra, metal. Adapted from ref. 30. Copyright 2024 Springer Nature.

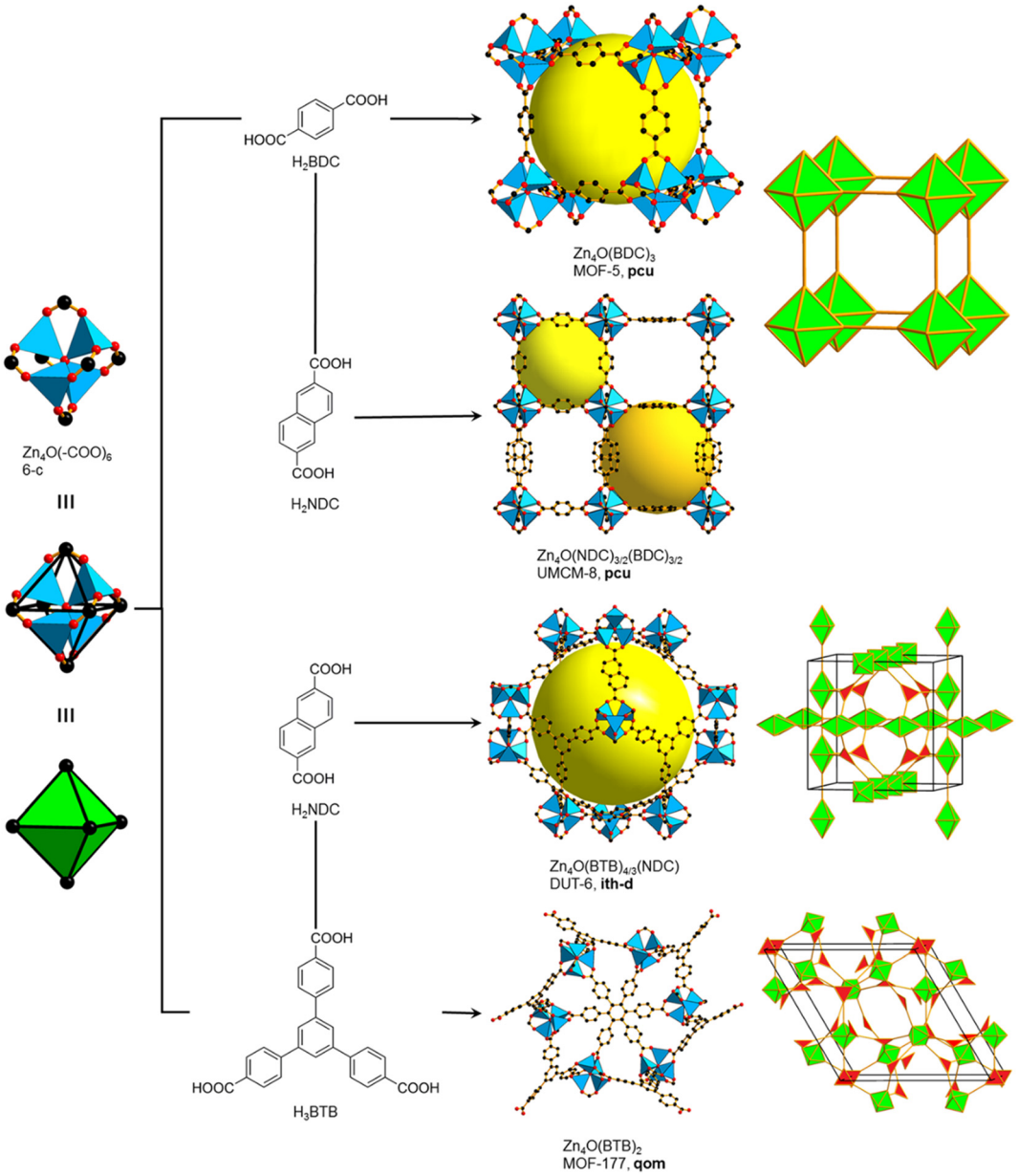

Fig. 3 MOFs constructed from $Zn_4O(–COO)_6$ SBUs. Color code: black, C; red, O; blue polyhedra, Zn. The yellow spheres represent the empty space in the framework. Hydrogen atoms are omitted for clarity. Adapted from ref. 30. Copyright 2024 Springer Nature.

length of the ligand, among others.[36] The inherent stability of a MOF is related to the strength of the coordination bond between the ligand and the metal cluster, making this an important factor to design MOFs. If this coordination bond is weak, the MOF will have a low lifetime and will have low thermal and chemical stability. One of the theories that help to predict the stability of the coordination bond in a MOF is the hard and soft acid and base (HSAB) theory.[37] In this theory, acids and bases are subclassified into soft and hard categories, which will depend on the polarizability of the molecular electronic cloud, where hard acids/bases have low polarizability, and soft acids/bases have high polarizability. This theory indicates that the bonding of an acid–base pair of the same category (soft–soft, hard–hard) will be more favorable than the bonding of acid–base pairs of different categories (soft–hard). Considering that there are carboxylate base linkers, where their deprotonated form, carboxylate ion ($–COO^-$), is the species that coordinates to the metal clusters, this theory applies to the formation of MOFs using these carboxylate ion polydentate ligands, which are considered hard bases. According to the HSAB theory, the carboxylate (hard base) binds favorably to transition metals of high oxidation states (>3+). In this sense, the linker benzene-1,4-dicarboxylate (from terephthalic acid) binds to metals such as Cr(III), Fe(III), Al(III) or Zr(IV), to form different MOFs such as MIL-88B(Fe), UIO-66, MIL-101(Cr), and MIL-53(Al), which have shown good thermal and chemical stability and have been applied as H_2 storage materials.[38–40] The HSAB theory is

useful to predict the stability that a MOF will have, since it predicts which metal–ligand bonds are more stable than others.

There are different methods in MOF preparation, such as solvothermal/hydrothermal, microwave, electrochemical, ultrasonic, mechanochemical, chemical flow, spray drying, *etc.*[20] We will highlight those that have been most commonly used and those that have the largest potential for large size synthesis. Each method has its advantages and disadvantages in MOF synthesis. Conventional synthesis methods, such as solvothermal methods, were initially proposed for MOF preparation. The solvothermal method consists of a stoichiometric mixture of the metal precursor and the organic ligand in an adequate organic solvent, in a hermetically sealed container (autoclave). If the used solvent is water, the method is called hydrothermal. The container is then heated in an oven at a certain temperature for a period of time. Under these conditions, the formation of MOF crystals occurs. This procedure has the advantage of being a single step method obtaining good yields. One of its disadvantages is its difficult to scale for large size synthesis, since the method considers many variables that must be parameterized, in addition to the use of large amounts of organic solvents and long synthesis times.[41] On the other hand, the microwave method is similar to the solvothermal method, but the energy source for the MOF's formation is microwave radiation. Microwave radiation helps to obtain MOFs in a shorter synthesis time compared to the solvothermal method, in addition to obtaining crystals with controllable particle sizes. However, currently this method is not scalable, due to the size of the required reactor and the requirement of large amounts of electricity.[42] Current synthesis methods seek to provide solutions to these problems of scalability in MOFs and have the characteristics of being easy and cheap to execute, such as the spray drying method.[43] The spray drying technique is a highly efficient method for synthesizing MOFs with precisely controlled particle sizes. This process involves atomizing a precursor solution into nano-sized droplets, which are then rapidly dried by a stream of hot gas. As the solvent evaporates, MOF particles begin to form, resulting in a uniform and well-defined morphology. One of the major advantages of this method is its ability to produce MOFs with consistent particle sizes, ensuring homogeneity in the final material.[44] Additionally, spray drying offers short preparation times, making it a time-efficient approach compared to traditional MOF synthesis methods. Furthermore, this technique is highly scalable, allowing large quantities of MOFs to be produced, which is crucial for industrial and commercial applications. A key factor in the success of spray drying is the appropriate formulation of the precursor solution. All necessary species, including metal salts and organic linkers, must be fully dissolved and well mixed to ensure uniform nucleation and particle formation. Careful optimization of solvent composition, temperature, and drying parameters is essential to achieve high-quality MOF structures with desirable properties for specific applications.[44,45] Another method is flow chemistry which specializes in having a constant inflow and outflow of reactants and products,[46,47] where the inflow contains the precursors, and the outflow contains the MOF that is formed inside the reactor. This method uses different continuous flow reactors, such as stirred tank reactors or plug flow reactors. The great advantages of this method are the easy control of the reaction parameters, where the concentration of the precursors, agitation of the reactor, and speed of the flows must be controlled since the necessary time must be given for the MOF formation to occur. This precise control also allows controlling the size of the particles, in addition to its scalability to obtain large quantities of MOFs. Since there are several MOFs that have shown promising applications as H_2 storage, it is essential to develop synthesis methodologies to obtain large quantities and test these MOFs in H_2 storage systems on a larger scale, therefore methods such as spray drying or flow reactors are good options for scalability of the MOFs, but there are no reports of MOF synthesis by spray drying and flow reactors methods applied to H_2 adsorption.

Open metal sites (OMSs)

Among the most promising strategies to enhance the affinity of MOFs for H_2, the incorporation of open metal sites (OMSs) stands out due to the strong interactions that OMSs provide with H_2 molecules. MOFs exhibit varying degrees of metal center coordination, which can be either fully coordinated or unsaturated, leading to structural defects such as missing organic linkers.[48–50] These OMSs enable the design of new binding sites (see Fig. 4), significantly expanding the range of applications for these materials, including catalysis, gas storage, and separation.[51–54] The generation of reactive OMSs in MOFs is one of the most attractive strategies, as they can create local environments similar to those of homogeneous catalysts. Moreover, the presence of OMSs in these porous materials enhances sorbent selectivity.[55,56]

By modifying the coordination of metal ions in the SBU of the material, the crystallinity and porosity of the structure

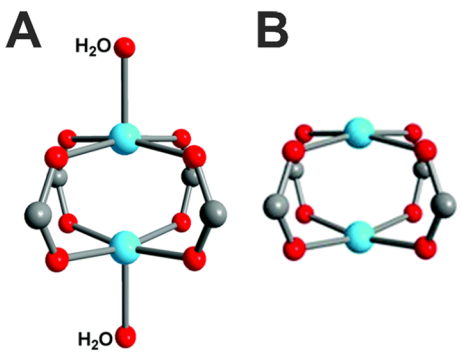

Fig. 4 SBU of HKUST-1. (A) HKUST-1 with water molecules after activation and (B) HKUST-1 activated with loss of water molecules giving rise to OMSs. Reproduced from ref. 57. Copyright 2024 Advanced Energy Materials.

must be maintained. During the synthesis of MOFs, vacant coordination sites are usually occupied by solvent molecules (labile ligands), which stabilize the structure by saturating the coordination sphere.

To generate OMSs, it is necessary to remove labile terminal ligands, which usually are synthesis molecules such as DMF, water, or alcohols.[58] Thus, different strategies are used for the generation of OMSs:

a) Solvent exchange and thermal activation: for example, a high-boiling solvent (DMF) is replaced with a more volatile solvent (acetone). Acetone molecules are then removed by thermal activation at low temperatures and high vacuum pressures.[59,60]

b) Chemical activation: this method consists of washing the MOF with volatile solvents, which are subsequently removed by air drying at room temperature.[61,62]

c) Photothermal activation: this method is applied to kinetically stable metal ions and uses UV-vis radiation to induce a photoactive excited state, facilitating the removal of ligands.[63]

Furthermore, once the OMSs are obtained, it is possible to quantify the percentage obtained in each material. The techniques used are gas adsorption techniques, temperature programmed desorption (TPD), and infrared spectroscopy using probe molecules such as H_2, CO_2, CO, and water.[64–66]

The presence of OMSs in MOFs allows the design of materials with specific interactions, which expands their functionality. Additionally, the stronger binding sites presented within the OMS-MOF structures enhance the interactions between H_2 and the material. In contrast, it has been demonstrated that when the metal center is fully coordinated (defect-free materials), the material has a low performance in H_2 adsorption and production.[67] This turns OMS-MOFs into highly promising materials for H_2 separation and storage.

The most commonly used secondary building units (SBUs) to generate open metal sites are bimetallic, where the solvent coordination at the available sites is in axial positions. There are different bimetallic materials used for H_2 production, such as MOF-74 with divalent OMSs, which has different isostructural derivatives, referred as MOF-74-M (M_2(dobdc), where M = Co, Cu, Mg, Mn, Ni and dobdc = 2,5-dioxide-1,4-benzenedicarboxylate). This MOF has the highest known OMS volumetric density. MOF-74-Ni exhibits low thermal stability, so the incorporation of bimetallic OMSs with Mg is necessary to stabilize the structure. In this case, it has been shown that materials with (Ni_xMg_{1-x})-MOF-74 (where "x" corresponds to the fraction of each metal) increase the H_2 production.[68] In 2015, Orcajo *et al.* studied the capacity of bimetallic MOF-74 for H_2 adsorption in the presence of OMSs. In this case, the highest adsorption capacity was attributed to materials containing bimetallic OMSs of Co and Ni. This was compared with monometallic MOF-74-Cu, which had a lower adsorption capacity due to its lower affinity for H_2.[69]

Open metal sites have been generated in HKUST-1, through synthesis methods, and increase the available surface area and intensify the interaction between the gas and the material.[70] However, the storage capacity of this material can vary significantly depending on the activation method and sample handling in the presence of open metal sites.[71–73]

On the other hand, Suh and his group compared the H_2 storage capacity in structural materials with and without OMSs, using MOFs with different amounts of these available sites (SNU-4, SNU-5, and SNU-5′). SNU-5 (SNU: Seoul National University), which presents open metal sites, showed a higher adsorption capacity.[74]

In every case, the OMSs produce an increase in the H_2 storage capability, as the generated interaction, often described as electrostatic attraction, results in a stronger binding strength compared to conventional MOFs (MOFs which do not possess OMSs). The presence of OMSs boosts the adsorption capacity of MOFs, allowing them to store more H_2 gas. This enhanced adsorption is attributed to the increased interaction strength between the metal sites and the H_2 molecules. Thus the generation of new MOFs with the possibility of having more OMSs is a current topic in research for adsorption materials.[74]

Linker modifications for H_2 affinity

Organic linkers are essential to the MOF structure since they contribute to determining the topology of the material, and by consequence, they play an important role in the properties and applications of MOFs. For H_2 industry applications, surface area is directly related to gas adsorption capacity, and thus the development of new MOFs with ultra-high surface area is being studied. One of the simplest ways to increase the surface area is to incorporate longer linkers to form isoreticular MOFs; this approach allows synthesis of MOFs with a similar crystalline structure but with different compositions.[75] However, there are two difficulties, (1) the large void generated could cause the interpenetration of the crystal frameworks as a form of structural stabilization (but occluding each other's pores) and (2) the incorporation of longer linkers decreases the crystal framework stability like the case of PCN-610 where the crystal structure collapsed after the removal of the solvent guest molecules.[76–81]

Zhou *et al.*[81] worked with a family of isoreticular MOFs based on dendritic hexacarboxylic acids with different lengths. The MOFs PCN-61, −66, −68 and −610 exhibited a BET surface area that increased with the linker's length from 3000 $m^2\ g^{-1}$ to 5109 $m^2\ g^{-1}$ in the case of PCN-68. However, the structure of PCN-610 completely collapsed during the activation process. On the other hand, Hupp *et al.*[82] synthesized NU-100 (the same as PCN-610, but NU-100 was successfully activated) with a BET surface area of 6143 $m^2\ g^{-1}$. The effect of a high surface area on the gas adsorption capacities for H_2 was studied for the mentioned PCN and NU MOFs. The H_2 uptake showed that in the low-pressure region, the sorption capacities are dominated by H_2 affinity, where PCN-61 had the highest isosteric heat due to

its reduced pore volume. The high pressure range is controlled by surface area and pore volume, so NU-100 exhibited a total gravimetric H_2 uptake of 164 mg g^{-1} at 70 bar and 77 K, and PCN-68 exhibited a total gravimetric H_2 uptake of 130 mg g^{-1}, followed by PCN-66 with an uptake of 110 mg g^{-1} and finally 90 mg g^{-1} for PCN-61 at 100 bar and 77 K. This trend becomes inverted when calculating the volumetric H_2 uptake capacities, where the MOFs exhibited a total volumetric uptake of approximately 48, 50 and 52 g L^{-1} at 100 bar and 77 K for PCN-66, PCN-68 and PCN-61, respectively. The inversion in trend is due to the volumetric capacities being dominated by the densities of the crystal framework.

These studies highlight the effect of elongating the linker on the H_2 uptake performance. As could be noted, the increase in surface area weakens the crystal structure and lowers the volumetric uptake. This hinders the application of MOFs for H_2 transportation where a balance between gravimetric and volumetric uptake is needed.[83]

On the other hand,[80] the use of two linkers to yield two new MOFs (MOF-180, MOF-200) with high surface areas was studied by Yaghi *et al.*;[80] the mixing of 4,4′,4″-benzene-1,3,5-triyl-tribenzoate (BTB)/2,6-naphthalenedicarboxylate (NDC) and 4,4′,4″-(benzene-1,3,5-triyl-tris(ethyne-2,1-diyl))tribenzoate (BTE)/biphenyl-4,4′-dicarboxylate (BPDC) linkers yielded MOF-205 and MOF-210, respectively. MOF-205 and MOF-210 exhibited a surface area of 4460 and 6240 m^2 g^{-1} and a total gravimetric H_2 uptake of 123 and 176 mg g^{-1} at ~60 bar and 77 K, respectively, see Table 1 (ref. 76) Moreover, the influence of the di- and tritopic linker length ratio (L_D/L_T) and mole fraction to yield UMCM-1, −2, −3, −4 and −5 was analyzed.[76] The mixture of different linkers has effects on the reactivity which requires a modification of the mole fraction in the synthetic feed, where tritopic linkers are consumed in the reaction statistically 1.5 times faster than ditopic linkers due to the presence of more carboxylic groups. Thus, an excess of the ditopic linker (compared with its presence in the framework) is needed to achieve pure copolymerization of the MOF. The UMCM-*X* series were successfully synthesized in mole ratios between 8 : 2 and 5 : 5. On the other hand, changes in L_D/L_T influence the connectivity of the linker to the cluster, constructing new structure types in some cases. According to known MOFs, the linker length

Table 1 Summary of MOFs with high H_2 adsorption capacities

MOF	Linker	Molecular formula	BET surface area [m^2 g^{-1}]	Total H_2 gravimetric uptake at 77 K[mg g^{-1}]	Total H_2 volumetric uptake at 77 K [L g^{-1}]	Topology	Synthesis method	Ref.
PCN-61	H_6BTEI	Cu_3(BTEI)$(H_2O)_3$	3000	90[a]	52[a]	rht	Solvothermal	81, 88, 89
PCN-66	H_6NTEI	Cu_3(NTEI)$(H_2O)_3$	4000	110[a]	48[a]	rht	Solvothermal	81, 88, 89
PCN-68	H_6PTEI	Cu_3(PTEI)$(H_2O)_3$	5109	130[a]	50[a]	rht	Solvothermal	81, 89
NU-100 /PCN-610	H_6TTEI	Cu_3(TTEI)$(H_2O)_3$	6143	164[c]	—	rht	Solvothermal	81, 82, 89
MOF-200	H_3BBC	$Zn_4O(BBC)_2(H_2O)_3$	4530	163[b]	36[b]	qom	Solvothermal	80
MOF-205	H_3BTB, H_2NDC	$Zn_4O(BTB)_{4/3}$(NDC)	4460	120[b]	46[b]	ith-d		
MOF-210	H_3BTE, H_2BPDC	$Zn_4O(BTE)_{4/3}$(BPDC)	6240	176[b]	44[b]	toz		
MOF-5	H_2BDC	$Zn_4O(BDC)_3$	3800	110[a]	66[a]	pcu	Solvothermal	80, 90
MOF-177	H_3BTB	$Zn_4O(BTB)_2$	4750	110[c]	47[c]	pyr	Solvothermal	91, 92
DUT-32	H_2BPDC, H_3BTCTB	Zn_4O(BPDC) $(BTCTB)_{4/3}$	6411	166[b]	—	umt	Solvothermal	93
NOTT-112	H_6L	Cu_3(L)$(H_2O)_3$	3800	100[c]	50[c]	rht	Solvothermal	94, 95
DUT-49	H_4BBCDC	Cu_2(BBCDC)	5476	165[a]	—	fcu	Solvothermal	96
NU-1500-Al	H_6PET	$Al_3(\mu_3\text{-}O)(H_2O)_2$(OH) (PET)	3560	89[a]	44.6[a]	acs	Solvothermal	83
NU-1501-Al	H_6PET-2	$Al_3(\mu_3\text{-}O)(H_2O)_2$(OH) (PET-2)	7310	170[a]	47.9[a]	acs		
NU-1501-Fe	H_6PET-2	$Fe_3(\mu_3\text{-}O)$ $(H_2O)_2$(OH)(PET-2)	7140	152[a]	45.4[a]	acs		
DUT-23(Co)	H_3BTB, BIPY	$[Co_2(BIPY)]_3(BTB)_4$	4850	~178[a]	40[a]	pto	Solvothermal	97
UMCM-2	H_2T^2DC, H_3BTB	$Zn_4O(T^2DC)(BTB)_{4/3}$	5200	68.8	—	umt	Solvothermal	98

[a] At 100 bar K. [b] At 80 bar. [c] 70 bar. H_6BTEI: 5,5′,5″-benzene-1,3,5-triyltris(1-ethynyl-2-isophthalic acid); H_6NTEI: 5,5′,5″-(4,4′,4″-nitrilotris(benzene-4,1-diyl)tris(ethyne-2,1-diyl))triisophthalic acid; H_6PTEI: 5,5′-((5′-(4-((3,5-dicarboxyphenyl)ethynyl)phenyl)-[1,1′:3′,1″-terphenyl]-4,4″-diyl)-bis(ethyne-2,1-diyl))diisophthalic acid; H_6TTEI: 5,5′,5″-(((benzene-1,3,5-triyltris(ethyne-2,1-diyl))tris(benzene-4,1-diyl))tris-(ethyne-2,1-diyl))triisophthalic acid; H_3BBC: 4,4′,4″-[benzene-1,3,5-triyl-tris(benzene-4,1-diyl)]tribenzoic acid; H_3BTB: 4,4′,4″-benzene-1,3,5-triyl-tribenzoic acid; H_2NDC: 2,6-naphthalenedicarboxylic acid; H_3BTE: 4,4′,4″-[benzene-1,3,5-triyltris(ethyne-2,1-diyl)]tribenzoic acid; H_2BPDC: biphenyl-4,4′-dicarboxylic acid; H_2BDC: 1,4-benzenedicarboxylic acid; H_3BTCTB: 4,4′,4″-[benzene-1,3,5-triyltris-(carbonylimino)]trisbenzoic acid; H_6L: 1,3,5-tris(3′,5′-dicarboxy[1,1′-biphenyl]-4-yl)benzene; H_4BBCDC: 9,9′-([1,1′-biphenyl]-4,4′-diyl)bis(9H-carbazole-3,6-dicarboxylic acid); H_6PET: see ref. 99; H_6PET-2: see ref. 100; BIPY: 4,4′-bipyridine; H_2T_2DC: thieno[3,2-b]thiophene-2,5-dicarboxylate.

ratio to generate a stable structure lies within a region from 0.44 to 0.66.[84]

The improvement in surface area of MOFs *via* linker elongation implies the framework debilitation, where a gentle activation with supercritical CO_2 helps to maintain the integrity of the crystal structure.[82,85] Linker elongation also increases the susceptibility of self-interpenetration, which is given on many cubic and tetrahedral networks, thus a topology selection or other techniques to avoid interpenetration could be considered.[80,85,86] Despite these difficulties, MOFs are near to achieve the on-board H_2 storage proposed by the U.S. Department of Energy for 2020 (4,5 wt%, 30 g L^{-1}, −40 to 60 °C, 5–12 bar) and for 2025 (5.5 wt%, 40 g L^{-1}, −40 to 60 °C, 5–12 bar).[87]

Another application of MOFs in the H_2 industry is their use as molecular sieves to purify H_2.[101,102]

In this context, Ghalei *et al.*[103] evaluated the effect of the bulkiness or functionality of organic linkers on the H_2 separation performance of isoreticular series of UiO-66 MOFs utilizing terephthalic acid (H_2BDC), 1,4-naphthalenedicarboxylic acid (H_2NDC), 9,10-anthracenedicarboxylic acid (H_2ADC), 2-amino-terephthalic acid ($H_2BDC\text{-}NH_2$) and 2-bromoterephthalic acid ($H_2BDC\text{-}Br$). In this work, it was observed that the bulkier organic ligands (H_2NDC and H_2ADC) significantly enhanced the H_2/CO_2 selectivity of separation to 15.3 and 31.9. Meanwhile for the H_2BDC linker (the less bulky linker), the H_2/CO_2 selectivity was 4.7, so it was concluded that the enhanced separation selectivity was induced by molecular sieving. Furthermore, the incorporation of functional groups did not change the H_2 separation properties.

Production of H_2 in MOFs by electrocatalysis

In line with efforts to develop more sustainable energy technologies, MOFs have demonstrated significant potential for H_2 production through electrocatalytic processes. H_2 production through water electrolysis positions this process as a key candidate for the transition to cleaner energy systems.[104] Electrolytic water splitting provides a viable and efficient method for alleviating energy shortages and reducing greenhouse gas emissions through a clean, safe, and straightforward process for H_2 production.[105] This process involves two electrocatalytic reactions: the H_2 evolution reaction (HER) occurring at the cathode and the oxygen evolution reaction (OER) taking place at the anode (see Fig. 5), requiring a theoretical voltage of 1.23 V.[106,107] The HER process is typically described as involving three steps: the Volmer step, where H_2O and an electron form H_{ad} and OH^-, followed by the H_2 formation, which can occur *via* the Heyrovsky step, where H_2O, H_{ad}, and an electron yield H_2 and OH^-, or through the Tafel step, where two H_{ad} atoms combine to produce H_2.[108–110]

The procedure is outlined in the equations below:

$$H_2O + e^- \rightarrow H_{ad} + OH^- \text{ (Volmer step)} \quad (1)$$

$$H_2O + H_{ad} + e^- \rightarrow H_2 + OH^- \text{ (Heyrovsky step)} \quad (2)$$

$$2\,H_{ad} \rightarrow H_2 \text{ (Tafel step)} \quad (3)$$

In recent decades, noble metals such as platinum (Pt), iridium (Ir), ruthenium (Ru), and rhodium (Rh) have been extensively studied as catalysts for the HER and OER. However, their high cost and limited availability pose significant barriers to widespread adoption in large-scale industrial applications.[111,112] This challenge underscores the importance of developing affordable and highly efficient electrocatalysts to advance electrocatalytic water splitting, a sustainable process for H_2 production and a promising pathway for clean energy generation.[113,114] MOFs are regarded as progress toward the practical use of solid catalysts in advanced industrial applications.[115] MOFs are distinguished by their unique electronic and structural properties, making them highly promising materials for electrocatalytic applications.[116]

Naik Shreyanka *et al.* reported three TM-MOFs known as M-BTC MOFs, where M represents Cu, Co, and Ni, and BTC refers to 1,3,5-benzenetricarboxylic acid, which showed improved electrocatalytic activity for water splitting.[117] Among these, the Co-BTC MOF demonstrated a H_2 production rate of approximately 332.9 μmol h^{-1}, highlighting its effectiveness as a catalyst for practical applications in sustainable fuel generation. X-ray photoelectron spectroscopy (XPS) analysis evidences mixed oxidation states of Co, Co^{2+} (781.30 eV) and Co^{3+} (783.08 eV). This performance of Co-BTC is primarily attributed to its structural properties, featuring unsaturated coordination sites. However, recent studies have highlighted metal node engineering as a highly effective approach for enhancing the electrocatalytic properties of MOF-based catalysts. Xudong Wen and Jingqi Guan[118] emphasized that integrating polymetallic components into MOFs represents a robust

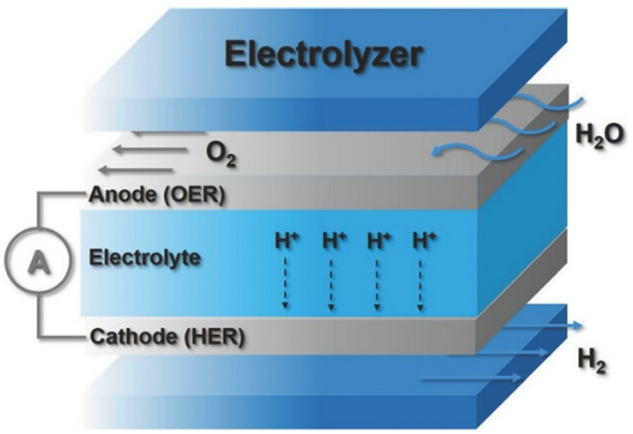

Fig. 5 Schematic representation of a water electrolyzer for electrocatalytic water splitting. Reproduced from ref. 107. Copyright 2024 John Wiley & Sons.

approach for electrocatalytic development of MOF-derived materials; a similar approach was used in other metal-based materials such as metallenes.[119] In this context, two main strategies have been explored: designing polymetallic MOFs composed of transition metal ions (TM-MOFs) and strategically doping TM-MOFs with noble metal species to achieve specific synergistic effects at the metal-centered active sites[120,121] Lin Yang *et al.*[122] reported an Fe-doped Ni-MOF, which showed efficiency and durability as an electrocatalyst for oxidizing water in alkaline medium. The Fe–Ni-MOF (labelled $Fe_{0.1}$–Ni-MOF/NF) showed an effectiveness for the oxygen evolution reaction (OER) in basic medium (1.0 M KOH solution), requiring low overpotentials of 243 and 263 mV to reach 50 and 100 mA cm^{-2}, respectively. It maintained its catalytic performance for over 20 hours at a high current density of 150 mA cm^{-2}. Additionally, it achieved high turnover frequency (TOF) values of 0.018 and 0.086 O_2 s^{-1} at overpotentials of 250 and 300 mV, respectively. The XPS spectrum showed the existence of the elements Fe, Ni, C, and O, indicating that Fe exists as Fe^{3+} and Ni as Ni^{2+}, respectively. This result suggests that MOFs based on Ni and Fe show potential as viable materials to generate electrode catalysts for water-splitting devices under alkaline conditions for large-scale H_2 production. This mixed-metal strategy within MOFs was also employed by Peng Cheng *et al.*[123] to synthesize a bimetallic family of Ni-NKU-101 MOFs. The isostructural bimetallic series, denoted as M_xNi_{1-x}-NKU-101 (X = 0.15, 0.19, 0.22 and 0.24), was prepared by partially substituting Ni centers with Mn, Co, Cu, or Zn ions. Among this series, the Cu/Ni-based systems exhibited the best HER performance. This work demonstrated that the metal ratio significantly influences the electrocatalytic HER activity. The XPS analysis revealed that the inclusions of Cu in Ni-NKU-101 induced an upshift of the electron density around the Cu centers due to their strong tendency to draw electrons from O and Ni atoms. This electron redistribution enhances the adsorption capacity of H_3O^+, thereby improving the HER performance.[123] Moreover, from this report it is suggested that the enhanced catalytic performance observed in bimetallic Cu–Ni MOFs can be further attributed to several synergistic factors. These include optimized H_2 binding sites resulting from the combined presence of Cu and Ni, tunable electronic properties achieved by varying the Cu–Ni ratio, and significantly increased surface area facilitated by Cu^{2+} ion exchange. These findings collectively highlight the potential of bimetallic MOFs as promising catalysts for various applications. In this context, Zhang *et al.*[124] synthesized a series of MOF-74-type frameworks based on Ce, Fe and Ni with organic ligand 2,5-dihydroxyterephthalic acid (DHTA) labeled Ce_xFeNi-MOF-74 (X = 0.50, 0.75, 0.86 and 0.90). These MOFs can be directly used as working electrodes. Among these materials, $Ce_{0.9}$-FeNi-MOF-74 exhibited superior electrocatalytic activity and stability towards both the HER and OER. XPS analysis revealed the presence of multiple oxidation states of the metals, suggesting synergistic interactions that contribute to the observed catalytic activity. This material achieved overpotentials of 257 mV and 262 mV at a current density of 100 mA cm^{-2} for the OER and HER, respectively. The reported performance can be considered as an excellent performance for this reaction. Moreover, $Ce_{0.9}$FeNi-MOF-74 demonstrated excellent stability with negligible voltage decay during a 60-hour continuous operation. This study demonstrates a novel approach for the rational design and synthesis of efficient water splitting polymetallic MOF-based electrocatalysts.

Along these lines, Yilin Wang *et al.*[125] reported that the incorporation of noble metals into bimetallic MOFs can profoundly modify their local electronic structure. This modification enhances the availability of active sites, refines the electronic configuration, and synergistically facilitates the adsorption and dissociation of intermediates, thereby significantly boosting the catalytic performance of the materials. The development of bimetallic MOFs is therefore needed to enhance the catalytic activity involved in both the HER and OER.

Jianrong Chen *et al.*[126] synthesized an FeCo-MOF doped with Ru, which showed a good performance in water electrolysis under alkaline conditions. XPS analysis confirmed the successful formation of Ru/FeCo-MOF catalysts. The author pointed out that doping of the FeCo-MOF with Ru enhanced the catalytic performance of the material. The inclusion of Ru introduces new active sites and tunes the electronic structure through interactions with Fe and Co. The $Ru_{0.04}$/FeCo-MOF configuration demonstrated superior activity, achieving a current density of 10 mA cm^{-2} with a voltage of only 1.498 V, surpassing RuO_2-based systems. This catalyst also exhibited excellent stability, maintaining 88.9% conversion after 8000 cycles. Notably, the nanosheet-stacked array structure provided a large active surface area and efficient ion exchange, leading to exceptional performance in both the OER (309 mV at 50 mA cm^{-2}) and HER (180 mV at 10 mA cm^{-2}) under alkaline conditions. Furthermore, the high surface capacitance of 8600 mF cm^{-2} underscores its potential in energy storage. These findings highlight a promising strategy for tailoring the morphology and electronic structure to develop advanced catalysts for energy conversion and storage applications.

Gugtapeh *et al.*[127] reported a composite material based on a bimetallic MOF (NiCo-MOF) combined with N-doped graphene quantum dots (NGQDs). The NGQD/NiCo-MOF composite was synthesized *via* a controlled electrodeposition strategy, resulting in a non-noble metal catalyst for alkaline water splitting. The synergy between Ni and Co ions enabled tuning of the electronic structure and an increase in active sites, while the uniform incorporation of NGQDs into the porous NiCo-MOF matrix enhanced local electrical conductivity. The composite exhibited outstanding electrochemical stability, sustaining HER and OER activities for more than 150 hours in 1 M KOH. Additionally, the two-electrode electrolyzer achieved overall water splitting with a low driving voltage of 1.62 V at a current density of 10 mA cm^{-2}. These exceptional electrochemical characteristics

underscore the promise of the NGQD/NiCo-MOF as an efficient MOF-based electrode material for H_2 electrocatalysts. Recent reports by Bin Zhao *et al.*[128] have introduced another class of MOF-based heterostructures, combining MXenes with TM-MOFs, resulting in efficient electrocatalysts for the OER. This composite electrocatalyst, obtained from Ni-doped Co-MOF-74 and $Ti_3C_2T_x$ MXene (denoted as CoNi-MOF-74/MXene/NF). This material exhibited exceptional performance for the OER, achieving a current density of 100 mA cm^{-2} at a low overpotential of just 256 mV, accompanied by a Tafel slope of 40.21 mV dec^{-1}. In HER catalysis, the CoNi-MOF-74/MXene/NF achieved a current density of 10 mA cm^{-2} at a remarkably low overpotential of 102 mV. Furthermore, a two-electrode electrolyzer utilizing the CoNi-MOF-74/MXene/NF as both the cathode and anode required only 1.49 V to achieve a current density of 10 mA cm^{-2}. These results highlight a promising approach for the development of high-performance bimetallic MOF-based electrocatalysts.

Wen Gu *et al.*[129] explored the catalytic performance of layered double hydroxides (LDHs) integrated with MOFs for the OER. They synthesized an FeNi LDH/MOF heterostructure *via* a two-step solvothermal method using an Fe-soc-MOF as the substrate, followed by Ru doping through a hydrothermal process. The incorporation of Ru was shown to significantly enhance electrochemical activity by modulating the electronic structure and facilitating electron transfer. The resulting material exhibited excellent performance, achieving a low overpotential of 242 mV at a current density of 10 mA cm^{-2} and demonstrating stable operation for 48 hours of continuous electrolysis. The high OER efficiency stems from the FeNi LDH/MOF heterostructure exposure of more active sites, with additional new active sites generated through Ru doping.

On the other hand, it is important to highlight that the working conditions could affect material stability. From the mentioned material, it was reported that the pH of the working conditions used to test co-BTC affects the integrity of the material. However, NiCo-UMOFN,[130] NiMn-MOF,[131] Ru@FeNi LDH/MOF, NGQD/NiCo MOF, FeCoMOF,[132] and $Ce_{0.9}$FeNi-MOF-74 do not present any perceptible change in their structure and catalytic capacity under working conditions. The above mentioned studies demonstrated that the tunability of MOFs is a huge advantage to improve the catalytic performance through the modulation of electronic interactions. The insights gained into bimetal non-noble metal MOFs underscore their versatility and promise for the next generation electrocatalysts in energy conversion applications. In addition, they underscore the potential of MOF-based composite materials as versatile platforms for catalytic applications, where their tunable structure and ability to integrate with diverse components enable the design of high-performance electrocatalysts for efficient and sustainable energy conversion processes.

Production of H_2 in MOFs by photocatalysis

The photocatalytic production of H_2 has been studied since the discovery of the water-splitting reaction in 1972. In this report, the water molecule broke into molecular H_2 and molecular oxygen in the presence of a TiO_2 electrode exposed to ultraviolet radiation.[133] This method of H_2 production has the advantage of using solar energy, making the process environmentally friendly.[134,135] However, this represents a limitation because most of the sunlight corresponds to the visible range of light. Consequently, the band gap of the semiconductor, used as a photocatalyst, must be narrow enough to absorb solar light efficiently.[136]

In general, the photocatalytic process to obtain H_2 has three main steps. The first one is the absorption of sunlight by the light-irradiated photocatalyst that generates the electronic excitation of the material, causing the transition of electrons from the valence band to the conduction band and the formation of holes in the valence band (known as the electron–hole pairs), which correspond to charge carriers.[135,137] The second step corresponds to the separation of electron–hole pairs and their independent migration to the photocatalyst's surface. The third step of this process consists of the reduction reaction of the electrons in the photocatalyst surface with water to produce H_2. Simultaneously, in the surface, the oxidation reactions occur between the holes and water or sacrificial reagents, denominated scavengers, improving the separation of the charge carriers.[137] Initially, some compounds, such as ZnO, TiO_2, $ZnIn_2S_4$, $Zn_2Ga_2O_4$, and CdS, were used as conventional photocatalysts in H_2 production. However, these materials have disadvantages, such as low solar energy harvest due to their large band gap and insufficient transport capacity of the photogenerated charge carriers, which cause fast recombination of electron–hole pairs and generate a photocatalytic process with low H_2 production. For this reason, it has been necessary to develop new semiconductor materials with efficient photocatalytic activity in H_2 production capable of overcoming the drawbacks mentioned above.[134,138] Thus, MOFs gain relevance due to the semiconductor characteristics of their structure, as the organic linkers act as an antenna able to absorb sunlight and transmit it to the metal clusters, where the redox reaction can occur.[139,140] Despite the advantages of the MOF structures, these materials present the inconvenience of having a large band gap value, thus showing absorption of light in the ultraviolet wavelength range.

According to the semiconductor character of the MOFs, it is possible to determine their band gap value by knowing the energy difference between the frontier molecular orbitals of the molecule, specifically, the highest occupied molecular orbital (HOMO) and the lowest unoccupied molecular orbital (LUMO).[75] Thus, the tunability of the MOF structure plays an important role because, through the incorporation of electronic donor groups, such as amino ($-NH_2$) or hydroxyl (–OH) in the linker, it's possible

to decrease the energy gap between the HOMO and the LUMO. Consequently, the band gap is shifted to lower values, which is associated with the absorption in the visible range of the solar spectrum. This band gap reduction helps MOFs to reach more efficient photocatalysts for H_2 production.[75,141] An example of the improvement in the photocatalytic properties of MOFs with the incorporation of linkers with electronic donor groups is the case of UiO-66 and UiO-66-NH_2. The first material (UiO-66) is known for showing no activity for the photocatalytic H_2 production in the visible range of light.[142] Meanwhile, UiO-66-NH_2 proved to be an active material for H_2 photocatalytic production with a mean production rate of 0.210 μmol gh^{-1} in the visible range of light.[136] Another example is the incorporation of fluor to the linker used to synthesize a Cu–NH_2 MOF. This approach demonstrated that the incorporation of fluor to the linker structure improves the photocatalytic performance of the material.[143]

Another employed methodology to achieve efficient H_2 production is by avoiding the recombination of electron–hole pairs through the generation of heterojunctions with MOFs. A heterojunction is the interface result of the union between two different semiconductor materials that can generate a band alignment, due to the similarity of the distinct band structure of each material[135] (see Fig. 6). Thus, a heterojunction resultant of the semiconductor material combination improves the separation of the charge carriers in the system, diminishing their recombination rate.[144] Focusing on this topic, several studies have been conducted on the different types of heterojunctions that involve MOF structures.

One of the band structures in the photocatalyst studied for H_2 production is the type II heterojunction, where the valence and conduction bands of both semiconductors are staggered. Thus, the photogenerated holes are transferred to the conduction band that has the less positive energy value, while the electrons are transferred to the conduction band with the less negative energy value.[146] An example of this type of material is the work realized by Chen *et al.*, which generated a semiconductor with a type II heterojunction between $ZnIn_2S_4$ and a MOF with copper metal centers, which was able to produce H_2 with a rate of 0.300 mmol gh^{-1}.[147] Also, the CdS/UiO-66-NH_2 heterojunction exhibited a H_2 evolution rate of 0.640 mmol gh^{-1}.[135] Meanwhile, the heterojunction formed between CuInZnS quantum dots and a nickel-based MOF developed by Deng *et al.* was able to generate H_2 with a rate of 2.642 mmol gh^{-1}.

Alternatives to type II heterojunctions are the Z-scheme and S-scheme. These two heterojunctions solve the low redox capacity of type II heterojunctions by retaining the electrons in the conduction band.[146,148] In the case of the Z-scheme, materials that include a porphyrin MOF combined with protonated carbon nitride[149] or $ZnIn_2S_4$ have been developed.[139] These combinations generated semiconductor materials with a photocatalytic H_2 production rate of 0.200 mmol gh^{-1} and 0.284 mmol gh^{-1}, respectively. In the case of the S-scheme, different studies have reported materials with heterojunctions, for example, some formed from ZnCdS/MOF-545Co (ref. 150) and Cu-MOF/$Cd_{0.5}Zn_{0.5}S$,[151] showing a H_2 production rate of 0.148 mmol h^{-1} and 18.986 mmol gh^{-1}, respectively.

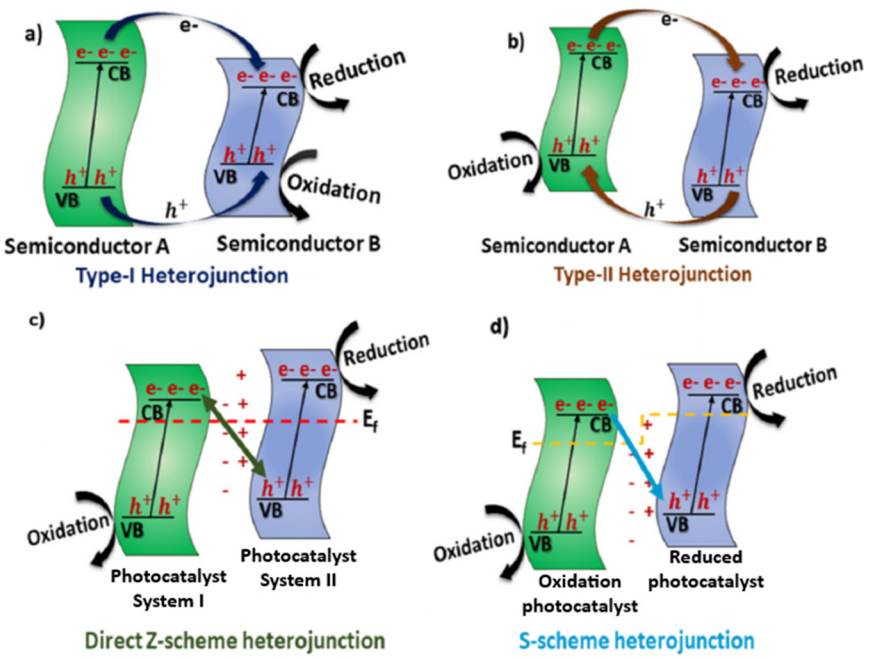

Fig. 6 Schematic representations of different types of heterojunctions. a) Type I heterojunction, b) type II heterojunction, c) direct Z-scheme heterojunction and d) S-scheme heterojunction. Modified from ref. 145. Copyright 2024 Elsevier.

Furthermore, the design of a ternary heterojunction has been studied. An example is that reported by Bi *et al.* who generated the photocatalytic composite NiS/CdS@DUT-67 with a H_2 production rate of 9.618 mmol gh^{-1}.[152] In this material, NiS and DUT-67 manage the electron flow direction in the heterojunction and the charge carrier separation during the photocatalysis, thus, they work as dual cocatalysts of CdS.[141,152] Besides, an engaging topic is the assembly of heterojunctions between MOFs, denominated MOF/MOF heterojunctions. This was studied using a semiconductor material formed from a MIL-167/MIL-125-NH_2 heterojunction. This material shows photocatalytic activity to produce H_2 with a rate of 0.455 mmol gh^{-1} that is a better performance than those of its single components (0.8 and 51.2 μmol gh^{-1} for MIL-167 and MIL-125-NH_2, respectively). To achieve this material, the authors used MOFs with comparable light absorption behavior and ensured the growth of one MOF in the presence of the other previously synthesized MOFs to ensure the correct electronic contact between the MOFs to generate the heterojunction.[153] Considering the concept of MOF/MOF heterojunctions, Ma *et al.* worked to generate a heterojunction made of two 2D-MOFs. Specifically, the material with a Ni-BDC/NiTCPP-3 heterojunction shows a photocatalytic H_2 production rate of 0.428 mmol g^{-1}.[154] It is worth mentioning that the stability of the material is a topic that needs to be more explored in the mentioned studies. From these, it is mentioned that the presence of TEOA (triethanolamine) as a scavenger affects the stability or activity of the material after long-term reactions.

Another interesting way to generate different types of heterojunctions is the use of MOFs as sacrificial templates, that means, generate semiconductors by calcining MOFs. Some examples of this methodology to obtain photocatalysts for H_2 production are the generation of a carbon-coated nickel phosphide (C-Ni_5P_4). This photocatalyst could be generated by calcining a Ni-MOF combined with a C-Ni_5P_4/CdS semiconductor and the calcination of ZIF-9 to originate CoP by a phosphating method to generate a CoP/In_2O_3 composite. The first one shows a H_2 production rate of 12.283 mmol gh^{-1},[155] while the CoP/In_2O_3 composite presents a total production of 0.251 mmol of H_2 in five hours.[137] Moreover, Ouyang *et al.* have reported the calcination of Co-MOF-74 to produce a Co_3O_4/CoO/Co_2P ternary heterojunction with a photocatalytic H_2 production rate of 6 mmol gh^{-1}.[156] Also, Musa *et al.* develop doped TiO_2 materials by calcining MIL-125-NH_2 obtaining a dual photocatalyst capable of producing H_2 with a rate of 0.329 mmol gh^{-1} and, at the same time, degrading pollutants in water as herbicides.[157]

MOFs used for H_2 storage

H_2 storage is the limiting step toward the application of H_2-powered fuel-cell vehicles and their global commercialization.[158] The current application of H_2 relies on compressed gas or liquefied gas, and both systems require the use of carbon fiber-reinforced tanks that are expensive and potentially unsafe.[159] To overcome these limitations, the current development of H_2 storage is guided by the directive of the US Department of Energy (DOE) which encourages the production of materials that can store 6.5 wt% and 50 g L^{-1} under operation conditions which are established as high pressure (5–100 bar) and low temperature (77–160 K). These conditions allow the utilization of an all-metal tank which is safe and practically inexpensive compared with the carbon fiber-reinforced tank.[160] Additionally, these conditions allow a range of work where H_2 can be adsorbed by the material at 100 bar and 77 K and desorbed at 5 bar and 160 K, generating a work window which represents the deliverable capacity of the developed material.

To date, several groups have studied the development of materials that can store H_2.[161–163] MOFs are highlighted in this field due to their high porosity, malleability, and stability. Considering the structure of MOFs, the topology, pore size, pore structure and metal composition (open metal sites) are the major aspects that impact their capacity to store H_2. In a previous study where the forms of the pore were compared, it was demonstrated that the cage-like form presents higher interactions between the material and the H_2 molecule than channel-like pores.[164] The size and form of the pore can be studied deeply through reticular chemistry. Reticular chemistry has been a key discipline to develop new MOF materials with improved H_2 adsorption capacity.[3,160] In this sense, the development of NU-1501 was achieved considering a rational design for the topology using an **acs**-a topology to obtain a material with a surface area of 7310 m^2 g^{-1}. This material presents a H_2 gravimetric adsorption capacity of 14 wt% and a volumetric working capacity of 46.2 g L^{-1}.[89] Furthermore, the application of reticular chemistry has guided different studies to explore different topologies *in silico* to identify possible materials that can store H_2 under the described working conditions. Through this theoretical approach, a study was conducted to analyze how the variation of its building blocks affects the H_2 adsorption of the **rht**-type MOF. From this approach, the authors identified the material PCN-61 which has a pore volume and volumetric surface area like MOF-5,[165] which is the best performance MOF material for H_2 storage described to date.

On the other hand, the variation of open metal sites has been studied. In a report that used experimental and theoretical approaches to evaluate MOF-74 using Ni^{2+}, Co^{2+} and Mg^{2+}, it was determined that Ni^{2+} presents the highest volumetric H_2 delivery capacity of 10.74 g L^{-1}. It is important to mention that MOF materials present low interaction capacity with the H_2 molecule at room temperature, due to the low polarizability of the H_2 molecule. To overcome this, the open metal sites in MOFs can be changed by a metal that increases the charge density in the OMSs, and thus can strongly polarize the H_2 molecule. The ideal range of isosteric heat of adsorption (Q_{st}) of H_2 in MOFs is estimated to be between −15 and −25 kJ mol^{-1}.[160] One example of the material developed to store H_2 at room temperature is NU-2100 prepared using Cu^+

which presents a delivery capacity of 10.4 g L^{-1} at 233 K/100 bar to 296 K/5 bar (ref. 166) with a Q_{st} of −15.7 kJ mol^{-1}. Another example is V_2Cl_2(btdd) which presents a Q_{st} of −20.9 kJ mol^{-1} and a delivery capacity of 26 g L^{-1} at 198 K/250 bar to 313 K/5 bar.[167] Finally, CuIZn-MFU-4 l presents a Q_{st} of −33.4 kJ mol^{-1} and a delivery capacity of 8.2 g L^{-1} at 298 K/100 bar to 298 K/5 bar.[168] Despite various efforts to improve MOF's H_2 storage capacity and delivery performance, there is still a long way to cover before these material can be applied in the H_2 storage system required for H_2-powered light vehicles. One of the decisive factors is to produce MOFs at an industrial scale with a performance and working conditions that meet the requirements set by the US DOE.[169,170]

Future of MOFs in the real life H_2 storage

As has been shown in the previous sections, MOFs have shown significant promise in H_2 storage applications due to their high surface areas, tunable pore sizes, and chemical functionalities. There are recent applications of MOFs in H_2 storage devices. As of now, there are limited commercial devices that utilize MOFs for this purpose. However, several notable recent developments highlight progress in this field. In this sense, H_2MOF is a startup co-founded in 2021 by Nobel laureate Sir Fraser Stoddart, along with Samer Taha and Omar Yaghi.[171] H_2MOF is a California-based startup dedicated to addressing challenges associated with H_2 storage and transportation using MOFs. The company focuses on developing MOF-based solutions to enhance H_2 storage efficiency. Specifically, the company aims to tackle challenges associated with H_2 storage and transportation by leveraging MOFs' ability to store H_2 at lower pressures and higher densities compared to conventional methods like compressed gas cylinders. Their approach focuses on designing next-generation MOFs that improve H_2 uptake efficiency, ensuring safer and more cost-effective storage. The startup's work aligns with global efforts to enhance H_2 infrastructure for fuel cell vehicles and industrial applications. Australian startup Rux Energy, in collaboration with the University of Sydney, is scaling up the manufacturing of advanced MOF materials for H_2 storage.[172] Their focus is on creating highly adsorbent, nanoporous MOFs that can significantly increase H_2 storage capacity in tanks. The project aims to develop field trial prototypes for use in heavy trucking and H_2 hubs, addressing the challenges of efficient H_2 storage in large-scale applications. This initiative represents a critical step toward practical, high-capacity H_2 storage solutions necessary for the widespread adoption of H_2 as a zero-carbon fuel. On the other hand, a program focused on engineering MOF composites aims to deliver densely packed, hierarchically porous materials with enhanced H_2 binding sites. These composites are designed to improve workable H_2 storage capacity and are processable through advanced manufacturing techniques for prototype development. The initiative includes testing H_2 storage capacity and resistance to embrittlement, with the goal of identifying promising materials for practical applications.

Furthermore, there have been computational advancements in MOF design, where recent studies employing Grand Canonical Monte Carlo simulations have evaluated the H_2 storage capacities of novel Al-nia MOFs at room temperature.[173] These simulations indicate that certain MOFs can achieve the Department of Energy's (DOE) H_2 storage targets, suggesting potential for future practical applications, which need to be experimentally supported. However, the ability to computationally predict MOF performance before synthesis accelerates material discovery, reducing the cost and time needed for experimental testing. There have been also developments of other multi-binding site covalent-organic frameworks (COFs). In this sense, research into COFs with multiple binding sites has shown promise for H_2 storage and delivery at room temperature.[174] These materials, related to MOFs, offer tunable structures that can be optimized for enhanced H_2 uptake, presenting a viable pathway toward efficient H_2 storage solutions. This breakthrough suggests that COFs, when optimized, could provide an alternative pathway to efficient H_2 storage for fuel cells and portable energy applications.

While these developments highlight significant progress, MOF-based H_2 storage solutions still face challenges related to cost, scalability, and long-term stability. However, ongoing research continues to push these materials toward commercial viability. With improvements in material synthesis, computational modeling, and industrial collaboration, MOFs could soon play a critical role in sustainable H_2 storage for transportation, aerospace, and grid energy applications.

Future research should prioritize a deeper understanding of MOF materials for hydrogen storage at ambient temperatures, as current MOFs exhibit very low hydrogen uptake capacities. Additionally, greater emphasis is needed on exploring cost-effective solvents and elucidating the catalytic mechanisms involved. Comprehensive analyses comparing the investment costs and economic feasibility of various hydrogen storage methods are also lacking and need further investigation. Advanced modeling studies that accurately reflect real-world conditions and complexities should be employed to enhance predictive capabilities. Despite progress, the discovery of stable, recyclable, and efficient MOF-based catalysts for low-cost water splitting remains a significant challenge. Therefore, continued research is essential before these technologies can be commercially deployed.

Data availability

There is no data besides the results provided in the article.

Conflicts of interest

There are no conflicts to declare.

Acknowledgements

The authors would like to acknowledge ANID/FONDAP/1523A0006, FONDECYT 1241917 and 1231194, and ANID Postdoctoral 3240414 and 3230141. This material is based upon work supported by the Air Force Office of Scientific Research under award number FA8655-25-1-8759.

References

1 R. Sule, A. K. Mishra and T. T. Nkambule, *Int. J. Energy Res.*, 2021, **45**, 12481–12499.
2 D. Zhao, X. Wang, L. Yue, Y. He and B. Chen, *Chem. Commun.*, 2022, **58**, 11059–11078.
3 J. Ren and D. Zhao, *Adv. Funct. Mater.*, 2024, **22**, 2307778.
4 AFHYPAC and FNCCR, *Déployer des stations hydrogène dans votre territoire*, 2024.
5 Environmental Protection Agency (EPA), *Inventory of U.S. Greenhouse Gas Emissions and Sinks: 1990–2023*, 2025.
6 P. N. R. Vennestrøm, C. M. Osmundsen, C. H. Christensen and E. Taarning, *Angew. Chem., Int. Ed.*, 2011, **50**, 10502–10509.
7 D. Mao, J. M. Griffin, R. Dawson, A. Fairhurst and N. Bimbo, *Int. J. Hydrogen Energy*, 2021, **46**, 23380–23405.
8 Q. Liu, Z. Li, D. Wang, Z. Li, X. Peng, C. Liu and P. Zheng, *Front. Chem.*, 2020, **8**, 694.
9 M. R. Usman, *Renewable Sustainable Energy Rev.*, 2022, **167**, 112743.
10 M. Simanullang and L. Prost, *Int. J. Hydrogen Energy*, 2022, **47**, 29808–29846.
11 M. D. Allendorf, V. Stavila, J. L. Snider, M. Witman, M. E. Bowden, K. Brooks, B. L. Tran and T. Autrey, *Nat. Chem.*, 2022, **14**, 1214–1223.
12 A. Y. Goren, M. Temiz, D. Erdemir and I. Dincer, *Energy*, 2025, **315**, 134257.
13 X. Hu, B. Guan, J. Chen, Z. Zhuang, C. Zheng, J. Zhou, T. Su, C. Zhu, S. Zhao, J. Guo, H. Dang, Y. Zhang, Y. Yuan, C. Yi, C. Xu, B. Xu, W. Zeng, Y. He, Z. Wei and Z. Huang, *Fuel*, 2025, **381**, 133134.
14 B. S. Solanki, H. Lim, S. J. Yoon, H. C. Ham, H. S. Park, H. E. Lee and S. H. Lee, *Renewable Sustainable Energy Rev.*, 2025, **207**, 114974.
15 B. Singh, A. Singh, A. Yadav and A. Indra, *Coord. Chem. Rev.*, 2021, **447**, 214144.
16 L. Wang and R. T. Yang, *Energy Environ. Sci.*, 2008, **1**, 268–279.
17 J. O. Abe, A. P. I. Popoola, E. Ajenifuja and O. M. Popoola, *Int. J. Hydrogen Energy*, 2019, **44**, 15072–15086.
18 C. Altintas and S. Keskin, *Mater. Today Energy*, 2023, **38**, 101426.
19 S. P. Shet, S. Shanmuga Priya, K. Sudhakar and M. Tahir, *Int. J. Hydrogen Energy*, 2021, **46**, 11782–11803.
20 P. Kumar, N. Kumar, D. Kumar and A. Editors, *Metal Organic Framework (MOFs) Catalytic Degradation of Pollutants*, 2024.
21 D. Yang and B. C. Gates, *ACS Catal.*, 2019, **9**, 1779–1798.
22 T. Jia, Y. Gu and F. Li, *J. Environ. Chem. Eng.*, 2022, **10**, 108300.
23 B. Hoskins and R. Robson, *J. Am. Chem. Soc.*, 1989, **111**, 5962–5964.
24 H. Li, M. Eddaoudi, M. O'Keeffe and O. M. Yaghi, *Nature*, 1999, **402**, 276–279.
25 A. Schoedel, in *Metal-Organic Frameworks for Biomedical Applications*, Elsevier, 2020, pp. 11–44.
26 V. Guillerm and M. Eddaoudi, *Acc. Chem. Res.*, 2021, **54**, 3298–3312.
27 X.-H. Bu, M. J. Zaworotko and Z. Zhang, *Metal-Organic Framework: From Design to Applications*, 2020.
28 J. Xing, L. Schweighauser, S. Okada, K. Harano and E. Nakamura, *Nat. Commun.*, 2019, **10**, 3608.
29 Q. Zhang, Y. Pramudya, W. Wenzel and C. Wöll, *Nanomaterials*, 2021, **11**, 1631.
30 A. Schoedel and S. Rajeh, *Top. Curr. Chem.*, 2020, **378**, 19.
31 Z. W. Zhu and Q. R. Zheng, *Int. J. Hydrogen Energy*, 2023, **48**, 5166–5174.
32 M. Eddaoudi, J. Kim, N. Rosi, D. Vodak, J. Wachter, M. O'Keeffe and O. M. Yaghi, *Science*, 2002, **295**, 469–472.
33 P. Ramirez-Vidal, R. L. S. Canevesi, A. Celzard and V. Fierro, *ACS Appl. Nano Mater.*, 2022, **5**, 759–773.
34 S. Shekhar and C. Chowdhury, *Mater. Adv.*, 2023, **5**, 820–830.
35 A. N. Hong, H. Yang, X. Bu and P. Feng, *EnergyChem*, 2022, **4**, 100080.
36 X. L. Lv, S. Yuan, L. H. Xie, H. F. Darke, Y. Chen, T. He, C. Dong, B. Wang, Y. Z. Zhang, J. R. Li and H. C. Zhou, *J. Am. Chem. Soc.*, 2019, **141**, 10283–10293.
37 A. M. Hamisu, A. Ariffin and A. C. Wibowo, *Inorg. Chim. Acta*, 2020, **511**, 119801.
38 M. Simani and H. Dehghani, *Fuel*, 2023, **341**, 127624.
39 Z. Xuan, Z. Qing-rong, H. Hong-zhou, S. Ting-quan and Z. Zhong-gang, *Int. J. Hydrogen Energy*, 2022, **47**, 9958–9968.
40 M. Simani and H. Dehghani, *Fuel*, 2024, **378**, 132942.
41 A. J. L. Pombeiro, K. T. Mahmudov and M. F. C. Guedes da Silva, *Synthesis and Applications in Chemistry and Materials*, World Scientific, 2024, vol. 11.
42 S. Głowniak, B. Szczęśniak, J. Choma and M. Jaroniec, *Adv. Mater.*, 2021, **2**, 2103477.
43 J. Troyano, C. Çamur, L. Garzón-Tovar, A. Carné-Sánchez, I. Imaz, D. Maspoch and D. Maspoch, *Acc. Chem. Res.*, 2020, **53**, 1206–1217.
44 N. Wang, Y. Wei, M. Chang, J. Liu and J.-X. Wang, *ACS Appl. Mater. Interfaces*, 2022, **14**, 10712–10720.
45 A. B. Albadarin, A. Metawea, M. Hammoud, M. N. Ahmad and G. Walker, *Microporous Mesoporous Mater.*, 2024, **372**, 113114.
46 S. Bagi, S. Yuan, S. Rojas-Buzo, Y. Shao-Horn and Y. Román-Leshkov, *Green Chem.*, 2021, **23**, 9982–9991.
47 D. Senthil Raja and D. H. Tsai, *Chem. Commun.*, 2024, **60**, 8497–8515.

48 J. G. Vitillo, L. Regli, S. Chavan, G. Ricchiardi, G. Spoto, P. D. C. Dietzel, S. Bordiga and A. Zecchina, *J. Am. Chem. Soc.*, 2008, **130**, 8386–8396.
49 M. Shöâeè, J. R. Agger, M. W. Anderson and M. P. Attfield, *CrystEngComm*, 2008, **10**, 646–648.
50 R. Ameloot, F. Vermoortele, J. Hofkens, F. C. De Schryver, D. E. De Vos and M. B. J. Roeffaers, *Angew. Chem., Int. Ed.*, 2013, **52**, 401–405.
51 M. H. Mohamed, Y. Yang, L. Li, S. Zhang, J. P. Ruffley, A. G. Jarvi, S. Saxena, G. Veser, J. K. Johnson and N. L. Rosi, *J. Am. Chem. Soc.*, 2019, **141**, 13003–13007.
52 Y. Xiao, Q. Guo, S. Yang, Q. Zhao and G. He, *ACS Sustainable Chem. Eng.*, 2024, **12**, 12446–12456.
53 M. Eddaoudi, H. Li and O. M. Yaghi, *J. Am. Chem. Soc.*, 2000, **122**, 1391–1397.
54 J. Bentley, G. S. Foo, M. Rungta, N. Sangar, C. Sievers, D. S. Sholl and S. Nair, *Ind. Eng. Chem. Res.*, 2016, **55**, 5043–5053.
55 M. H. Mohamed, Y. Yang, L. Li, S. Zhang, J. P. Ruffley, A. G. Jarvi, S. Saxena, G. Veser, J. K. Johnson and N. L. Rosi, *J. Am. Chem. Soc.*, 2019, **141**, 13003–13007.
56 S. T. Meek, J. A. Greathouse and M. D. Allendorf, *Adv. Mater.*, 2011, **23**, 249–267.
57 Ü. Kökçam-Demir, A. Goldman, L. Esrafili, M. Gharib, A. Morsali, O. Weingart and C. Janiak, *Chem. Soc. Rev.*, 2020, **49**, 2751–2798.
58 D. M. Chen, J. Y. Tian, C. Sen Liu and M. Du, *Chem. Commun.*, 2016, **52**, 8413–8416.
59 H. Woo, A. M. Devlin and A. J. Matzger, *J. Am. Chem. Soc.*, 2023, **145**, 18634–18641.
60 A. J. Rieth, Y. Tulchinsky and M. Dincă, *J. Am. Chem. Soc.*, 2016, **138**, 9401–9404.
61 H. K. Kim, W. S. Yun, M. B. Kim, J. Y. Kim, Y. S. Bae, J. D. Lee and N. C. Jeong, *J. Am. Chem. Soc.*, 2015, **137**, 10009–10015.
62 J. Bae, E. J. Lee and N. C. Jeong, *Chem. Commun.*, 2018, **54**, 6458–6471.
63 J. Espín, L. Garzón-Tovar, A. Carné-Sánchez, I. Imaz and D. Maspoch, *ACS Appl. Mater. Interfaces*, 2018, **10**, 9555–9562.
64 J. N. Hall and P. Bollini, *Langmuir*, 2020, **36**, 1345–1356.
65 J. N. Hall and P. Bollini, *React. Chem. Eng.*, 2019, **4**, 207–222.
66 Z. Hu and D. Zhao, *CrystEngComm*, 2017, **19**, 4066–4081.
67 P. Song, Y. Li, B. He, J. Yang, J. Zheng and X. Li, *Microporous Mesoporous Mater.*, 2011, **142**, 208–213.
68 J. L. Snider, J. Su, P. Verma, F. El Gabaly, J. D. Sugar, L. Chen, J. M. Chames, A. A. Talin, C. Dun, J. J. Urban, V. Stavila, D. Prendergast, G. A. Somorjai and M. D. Allendorf, *J. Mater. Chem. A*, 2021, **9**, 10869–10881.
69 G. Orcajo, J. A. Villajos, C. Martos, J. Á. Botas and G. Calleja, *Adsorption*, 2015, **21**, 589–595.
70 S. S.-Y. Chui, S. M.-F. Lo, J. P. H. Charmant, A. G. Orpen and I. D. Williams, *Science*, 1999, **283**, 1148–1150.
71 J. L. C. Rowsell and O. M. Yaghi, *J. Am. Chem. Soc.*, 2006, **128**, 1304–1315.
72 B. Panella, M. Hirscher, H. Pütter and U. Müller, *Adv. Funct. Mater.*, 2006, **16**, 520–524.
73 J. Lee, J. Li and J. Jagiello, *J. Solid State Chem.*, 2005, **178**, 2527–2532.
74 Y. G. Lee, H. R. Moon, Y. E. Cheon and M. P. Suh, *Angew. Chem., Int. Ed.*, 2008, **47**, 7741–7745.
75 S. Li, S. Sun, H. Wu, C. Wei and Y. Hu, *Catal. Sci. Technol.*, 2018, **8**, 1696–1703.
76 K. Koh, A. G. Wong-Foy and A. J. Matzger, *J. Am. Chem. Soc.*, 2010, **132**, 15005–15010.
77 X. Lin, J. Jia, P. Hubberstey, M. Schröder and N. R. Champness, *CrystEngComm*, 2007, **9**, 438–448.
78 J. K. Schnobrich, K. Koh, K. N. Sura and A. J. Matzger, *Langmuir*, 2010, **26**, 5808–5814.
79 B. Chen, M. Eddaoudi, S. T. Hyde, M. O'keeffe and O. M. Yaghi, *Science*, 2001, **291**, 1021–1023.
80 H. Furukawa, N. Ko, Y. B. Go, N. Aratani, S. B. Choi, E. Choi, A. Ö. Yazaydin, R. Q. Snurr, M. O'Keeffe, J. Kim and O. M. Yaghi, *Science*, 2010, **329**, 424–428.
81 D. Yuan, D. Zhao, D. Sun and H. Zhou, *Angew. Chem., Int. Ed.*, 2010, **49**, 5357–5361.
82 O. K. Farha, A. Ö. Yazaydin, I. Eryazici, C. D. Malliakas, B. G. Hauser, M. G. Kanatzidis, S. T. Nguyen, R. Q. Snurr and J. T. Hupp, *Nat. Chem.*, 2010, **2**, 944–948.
83 Z. Chen, P. Li, R. Anderson, X. Wang, X. Zhang, L. Robison, L. R. Redfern, S. Moribe, T. Islamoglu, D. A. Gómez-Gualdrón, T. Yildirim, J. F. Stoddart and O. K. Farha, *Science*, 2020, **368**, 297–303.
84 R. Grünker, V. Bon, P. Müller, U. Stoeck, S. Krause, U. Mueller, I. Senkovska and S. Kaskel, *Chem. Commun.*, 2014, **50**, 3450–3452.
85 K. O. Kirlikovali, S. L. Hanna, F. A. Son and O. K. Farha, *ACS Nanosci. Au*, 2023, **3**, 37–45.
86 R. P. Ojha, P. A. Lemieux, P. K. Dixon, A. J. Liu and D. J. Durian, *Nature*, 2004, **427**, 521–523.
87 DOE Technical Targets for Onboard Hydrogen Storage for Light-Duty Vehicles.
88 D. Zhao, D. Yuan, D. Sun and H. C. Zhou, *J. Am. Chem. Soc.*, 2009, **131**, 9186–9188.
89 Z. Chen, K. O. Kirlikovali, P. Li and O. K. Farha, *Acc. Chem. Res.*, 2022, **55**, 579–591.
90 S. S. Kaye, A. Dailly, O. M. Yaghi and J. R. Long, *J. Am. Chem. Soc.*, 2007, **129**, 14176–14177.
91 H. Furukawa, M. A. Miller and O. M. Yaghi, *J. Mater. Chem.*, 2007, **17**, 3197–3204.
92 H. K. Chae, D. Y. Siberio-Pérez, J. Kim, Y. Go, M. Eddaoudi, A. J. Matzger, M. O'Keeffe and O. M. Yaghi, *Nature*, 2004, **427**, 523–527.
93 R. Grünker, V. Bon, P. Müller, U. Stoeck, S. Krause, U. Mueller, I. Senkovska and S. Kaskel, *Chem. Commun.*, 2014, **50**, 3450–3452.
94 Y. Yan, X. Lin, S. Yang, A. J. Blake, A. Dailly, N. R. Champness, P. Hubberstey and M. Schröder, *Chem. Commun.*, 2009, 1025–1027.
95 J. Glover and E. Besley, *Phys. Chem. Chem. Phys.*, 2018, **20**, 23616–23624.
96 U. Stoeck, S. Krause, V. Bon, I. Senkovska and S. Kaskel, *Chem. Commun.*, 2012, **48**, 10841–10843.

97 N. Klein, I. Senkovska, I. A. Baburin, R. Grünker, U. Stoeck, M. Schlichtenmayer, B. Streppel, U. Mueller, S. Leoni, M. Hirscher and S. Kaskel, *Chem. – Eur. J.*, 2011, **17**, 13007–13016.
98 K. Koh, A. G. Wong-Foy and A. J. Matzger, *J. Am. Chem. Soc.*, 2009, **131**, 4184–4185.
99 P. Li, P. Li, M. R. Ryder, Z. Liu, C. L. Stern, O. K. Farha and J. F. Stoddart, *Angew. Chem., Int. Ed.*, 2019, **58**, 1664–1669.
100 Z. Chen, P. Li, X. Wang, K. I. Otake, X. Zhang, L. Robison, A. Atilgan, T. Islamoglu, M. G. Hall, G. W. Peterson, J. F. Stoddart and O. K. Farha, *J. Am. Chem. Soc.*, 2019, **141**, 12229–12235.
101 D. Mao, J. M. Griffin, R. Dawson, A. Fairhurst and N. Bimbo, *Int. J. Hydrogen Energy*, 2021, **46**, 23380–23405.
102 D. W. Lim, J. Ha, Y. Oruganti and H. R. Moon, *Mater. Chem. Front.*, 2021, **5**, 4022–4041.
103 B. Ghalei, K. Wakimoto, C. Y. Wu, A. P. Isfahani, T. Yamamoto, K. Sakurai, M. Higuchi, B. K. Chang, S. Kitagawa and E. Sivaniah, *Angew. Chem.*, 2019, **131**, 19210–19216.
104 R. Bhandari and N. Adhikari, *Int. J. Hydrogen Energy*, 2024, **82**, 923–951.
105 S. Alam, M. Jamil, M. Z. Iqbal, M. W. Khan, A. Khizar, A. M. Fouda, H. H. Hegazy, F. Alam and M. I. Saleem, *Mater. Chem. Phys.*, 2024, **322**, 129553.
106 S. Gong, Y. Meng, Z. Jin, H.-Y. Hsu, M. Du and F. Liu, *ACS Catal.*, 2024, **14**, 14399–14435.
107 B. Zhu, R. Zou and Q. Xu, *Adv. Energy Mater.*, 2018, **8**, 1–33.
108 K. Ao, Q. Wei and W. A. Daoud, *ACS Appl. Mater. Interfaces*, 2020, **12**(30), 33595–33602.
109 S. Zhang, *Chem. Soc. Rev.*, 2015, **44**, 2060–2086.
110 Z. Zhu, H. Yin, C. He, M. Al-mamun, P. Liu, L. Jiang, Y. Zhao, Y. Wang, H. Yang, Z. Tang, D. Wang, X. Chen and H. Zhao, *Adv. Mater.*, 2018, **30**, 1–7.
111 S. Gong, Y. Meng, Z. Jin, H.-Y. Hsu, M. Du and F. Liu, *ACS Catal.*, 2024, **14**, 14399–14435.
112 J. Wang, B. Yan, B. Fang and Z. Jian, *Mater. Lett.*, 2023, **332**, 133448.
113 J. Chen, G. Xia, P. Jiang, Y. Yang, R. Li, R. Shi, J. Su and Q. Chen, *ACS Appl. Mater. Interfaces*, 2016, **8**, 13378–13383.
114 X. Ding, D. Liu, P. Zhao, X. Chen, H. Wang, F. E. Oropeza, G. Gorni, M. Barawi, M. García-Tecedor, V. A. de la Peña O'Shea, J. P. Hofmann, J. Li, J. Kim, S. Cho, R. Wu and K. H. L. Zhang, *Nat. Commun.*, 2024, **15**, 5336.
115 S. Khan, T. Noor, N. Iqbal and E. Pervaiz, *ChemNanoMat*, 2022, **8**, e202200115.
116 A. Radwan, H. Jin, D. He and S. Mu, *Design Engineering, Synthesis Protocols, and Energy Applications of MOF - Derived Electrocatalysts*, Springer Singapore, 2021, vol. 13.
117 S. Naik Shreyanka, J. Theerthagiri, S. J. Lee, Y. Yu and M. Y. Choi, *Chem. Eng. J.*, 2022, **446**, 137045.
118 X. Wen and J. Guan, *Appl. Mater. Today*, 2019, **16**, 146–168.
119 S. Sanati, Q. Wang, R. Abazari and M. Liu, *Chem. Commun.*, 2024, **60**, 3129–3137.
120 X. Zhang, J. Luo, K. Wan, D. Plessers, B. Sels, J. Song, L. Chen, T. Zhang, P. Tang, J. R. Morante, J. Arbiol and J. Fransaer, *J. Mater. Chem. A*, 2019, **7**, 1616–1628.
121 S. Li, Y. Gao, N. Li, L. Ge, X. Bu and P. Feng, *Energy Environ. Sci.*, 2021, **14**, 1897–1927.
122 L. Yang, G. Zhu, H. Wen, X. Guan, X. Sun, H. Feng, W. Tian, D. Zheng, X. Cheng and Y. Yao, *J. Mater. Chem. A*, 2019, **7**, 8771–8776.
123 R. Zhang, L. Lu, Z. Chen, X. Zhang, B. Wu, W. Shi and P. Cheng, *Chem. – Eur. J.*, 2022, **28**, 1–7.
124 J. Zhang, T. Long, Y. Liu, Z. Zhong, Y. Zhang, X. Chen and G. Li, *Ionics*, 2025, **31**, 1937–1946.
125 Y. Wang, Y. Du, Z. Fu, M. Wang, Y. Fu, B. Li and L. Wang, *Int. J. Hydrogen Energy*, 2023, **48**, 23412–23424.
126 C. Feng, Q. An, Q. Zhang, L. Huang, N. Wang, X. Zhang, Y. Xu, M. Xie, R. Wang, Y. Jiao and J. Chen, *Int. J. Hydrogen Energy*, 2024, **55**, 189–198.
127 H. Shooshtari Gugtapeh and M. Rezaei, *ACS Appl. Nano Mater.*, 2024, **7**, 2086–2099.
128 K. Yu, J. Zhang, Y. Hu, L. Wang, X. Zhang and B. Zhao, *Catalysts*, 2024, **14**, 184.
129 Y. Cao, Y. Wen, Y. Li, M. Cao, B. Li, Q. Shen and W. Gu, *Dalton Trans.*, 2024, **53**, 5291–5300.
130 S. Zhao, Y. Wang, J. Dong, C. T. He, H. Yin, P. An, K. Zhao, X. Zhang, C. Gao, L. Zhang, J. Lv, J. Wang, J. Zhang, A. M. Khattak, N. A. Khan, Z. Wei, J. Zhang, S. Liu, H. Zhao and Z. Tang, *Nat. Energy*, 2016, **1**, 16184.
131 W. Cheng, X. F. Lu, D. Luan and X. W. Lou, *Angew. Chem., Int. Ed.*, 2020, **59**, 18234–18239.
132 J. Q. Shen, P. Q. Liao, D. D. Zhou, C. T. He, J. X. Wu, W. X. Zhang, J. P. Zhang and X. M. Chen, *J. Am. Chem. Soc.*, 2017, **139**, 1778–1781.
133 A. Fujishima and K. Honda, *Nature*, 1972, **238**, 37–38.
134 T.-T. Li, Y. Chen, Y. Cheng, M.-Q. Zheng, J.-F. Qian, M.-Y. He, Q. Chen and Z.-H. Zhang, *Int. J. Hydrogen Energy*, 2024, **65**, 225–235.
135 Y. Wang, L. Gudiño, J. Bedia and C. Belver, *Sep. Purif. Technol.*, 2025, **353**, 128663.
136 L. Gudiño, M. Peñas-Garzón, J. J. Rodriguez, J. Bedia and C. Belver, *Catal. Commun.*, 2024, **187**, 106858.
137 X. Jiang, M. Li, H. Li and Z. Jin, *Mol. Catal.*, 2021, **507**, 111551.
138 S. Xu, M. Li, Z. Li, M. Ding, Y. Wang and Z. Jin, *Int. J. Hydrogen Energy*, 2024, **70**, 666–676.
139 P. Jin, L. Wang, X. Ma, R. Lian, J. Huang, H. She, M. Zhang and Q. Wang, *Appl. Catal., B*, 2021, **284**, 119762.
140 Y. Hidalgo-Rosa, M. Saavedra-Torres, B. D. Koivisto, M. A. Treto-Suárez, D. Páez-Hernández, X. Zarate and E. Schott, *Inorg. Chem. Commun.*, 2025, **172**, 113635.
141 W. Cheng, S. Zhang, J. Wang, J. Yang, Z. Yang, X. Chen, J. Xiao and J. Wang, *Chem. – Eur. J.*, 2024, **30**, e202303886.
142 Y.-P. Yuan, L.-S. Yin, S.-W. Cao, G.-S. Xu, C.-H. Li and C. Xue, *Appl. Catal., B*, 2015, **168–169**, 572–576.
143 R. Abazari, S. Sanati, N. Li and J. Qian, *Inorg. Chem.*, 2023, **62**, 18680–18688.

144 J. Cai, B. Liu, S. Zhang, L. Wang, Z. Wu, J. Zhang and B. Cheng, *J. Mater. Sci. Technol.*, 2024, **197**, 183–193.
145 A. Shabbir, S. Sardar and A. Mumtaz, *J. Alloys Compd.*, 2024, **1003**, 175683.
146 D. Salazar-Marín, G. Oza, J. A. D. Real, A. Cervantes-Uribe, H. Pérez-Vidal, M. K. Kesarla, J. G. T. Torres and S. Godavarthi, *Appl. Surf. Sci. Adv.*, 2024, **19**, 100536.
147 H. Chen, J. Wu, Y. Zhu, J. Yang, B. Tang, T. Zhang and H. Yang, *Renewable Energy*, 2024, **228**, 120672.
148 H. Li, H. Gong and Z. Jin, *Appl. Catal., B*, 2022, **307**, 121166.
149 W. Zhu, L. Qin, Z. Ou, J. Tao, T. Zhang, S. Z. Kang and X. Li, *Fuel*, 2024, **376**, 132665.
150 M. Chen, K. Umer, B. Li, Z. Li, K. Li, W. Sun and Y. Ding, *J. Colloid Interface Sci.*, 2024, **653**, 380–389.
151 P. Zhu, C. Feng, Q. Liang, M. Zhou, Z. Li and S. Xu, *Ceram. Int.*, 2023, **49**, 20706–20714.
152 Y. Bi, K. Xu, Y. Wang, X. Li, X. Zhang, J. Wang, Y. Zhang, Q. Liu and Q. Fang, *J. Colloid Interface Sci.*, 2024, **661**, 501–511.
153 S. Kampouri, F. M. Ebrahim, M. Fumanal, M. Nord, P. A. Schouwink, R. Elzein, R. Addou, G. S. Herman, B. Smit, C. P. Ireland and K. C. Stylianou, *ACS Appl. Mater. Interfaces*, 2021, **13**, 14239–14247.
154 Y. Ma, H.-X. Fang, R. Chen, Q. Chen, S.-J. Liu, K. Zhang and H.-J. Li, *Rare Met.*, 2023, **42**, 3993–4004.
155 L. Luo, Y. Dang, J. Tian, K. Lin, D. Feng, W. Wang and B. Ma, *J. Colloid Interface Sci.*, 2024, **669**, 569–577.
156 Y. S. Ouyang and Q. Y. Yang, *J. Colloid Interface Sci.*, 2023, **644**, 346–357.
157 E. N. Musa, S. Kaur, T. C. Gallagher, T. M. Anthony, W. F. Stickle, L. Árnadóttir and K. C. Stylianou, *ACS Catal.*, 2023, **13**, 3710–3722.
158 J. Ren, H. W. Langmi, B. C. North and M. Mathe, *Int. J. Energy Res.*, 2015, **39**, 607–620.
159 Q. Cheng, R. Zhang, Z. Shi and J. Lin, *Int. J. Lightweight Mater. Manuf.*, 2024, **7**, 269–284.
160 Z. Chen, K. O. Kirlikovali, K. B. Idrees, M. C. Wasson and O. K. Farha, *Chem*, 2022, **8**, 693–716.
161 L. Ruihan, H. Feng, X. Ting, L. Yongzhi, Z. Xin and Z. Jiaqi, *Int. J. Hydrogen Energy*, 2024, **56**, 1079–1091.
162 W. Jiang, H. Wang and M. Zhu, *Rare Met.*, 2021, **40**, 3337–3356.
163 Y.-F. Zhang and J. Guo, *Int. J. Hydrogen Energy*, 2024, **50**, 1004–1014.
164 X. Zhang, R. B. Lin, J. Wang, B. Wang, B. Liang, T. Yildirim, J. Zhang, W. Zhou and B. Chen, *Adv. Mater.*, 2020, **32**, 1907995.
165 K. Liu, Z. Chen, T. Islamoglu, S. J. Lee, H. Chen, T. Yildirim, O. K. Farha and R. Q. Snurr, *J. Phys. Chem. C*, 2024, **128**, 7435–7446.
166 D. Sengupta, P. Melix, S. Bose, J. Duncan, X. Wang, M. R. Mian, K. O. Kirlikovali, F. Joodaki, T. Islamoglu, T. Yildirim, R. Q. Snurr and O. K. Farha, *J. Am. Chem. Soc.*, 2023, **145**, 20492–20502.
167 D. E. Jaramillo, H. Z. H. Jiang, H. A. Evans, R. Chakraborty, H. Furukawa, C. M. Brown, M. Head-Gordon and J. R. Long, *J. Am. Chem. Soc.*, 2021, **143**, 6248–6256.
168 Y. Yabuuchi, H. Furukawa, K. M. Carsch, R. A. Klein, N. V. Tkachenko, A. J. Huang, Y. Cheng, K. M. Taddei, E. Novak, C. M. Brown, M. Head-Gordon and J. R. Long, *J. Am. Chem. Soc.*, 2024, **146**, 22759–22776.
169 P. Peng, H. Z. H. Jiang, S. Collins, H. Furukawa, J. R. Long and H. Breunig, *ACS Energy Lett.*, 2024, **9**, 2727–2735.
170 M. T. Kapelewski, T. Runčevski, J. D. Tarver, H. Z. H. Jiang, K. E. Hurst, P. A. Parilla, A. Ayala, T. Gennett, S. A. FitzGerald, C. M. Brown and J. R. Long, *Chem. Mater.*, 2018, **30**, 8179–8189.
171 **https://h2mof.com/**.
172 **https://ruxenergy.com/**.
173 A. Granja-DelRío and I. Cabria, *Int. J. Hydrogen Energy*, 2024, **50**, 685–696.
174 M. Djokic and J. L. Mendoza-Cortes, *Energy Fuels*, 2024, **38**, 4711–4720.